May 27th, 2020
I.F.E.A. – Jean-Marie Laurichesse Research Award Committee

I.F.E.A. – Jean-Marie Laurichesse Research Award
Research Report

Astroglial Plasticity within the Rat Orofacial Primary Motor Cortex Induced by Endodontic Treatment *versus* Tooth Extraction

Acknowledgements

This work was funded by the Faculty of Dentistry Bertha Rosenstadt Fund, the American Association of Endodontists Foundation, the Canadian Academy of Endodontics Endowment Fund, International College of Prosthodontists, Shimon Friedman and Calvin Torneck Research Fund and International Federation of Endodontic Associations (I.F.E.A.) Jean-Marie Laurichesse Research Award.

Abstract

Objective: To optimise the CLARITY technique that renders brain tissue optically transparent, followed by immunolabelling and light sheet microscopy for 3D-characterisation of astroglial and neuronal cytoarchitecture and morphology within the rat orofacial primary motor cortex, and quantify changes in astroglia morphology following endodontic *versus* tooth extraction treatment.
Methods: Rats received either tooth extraction or endodontic treatment of the right maxillary molars, sham operation or no treatment. After one week, 2 mm-thick brain sections of the orofacial motor cortex were cleared and immunolabelled with astroglial and neuronal markers. 3D-images were acquired for characterisation and quantification of morphological features of astroglial processes.
Results: As compared with endodontic-, sham- and no-treatment, tooth extraction produced significantly thinner and straighter astroglial processes within layer-I of a laminar motor cortex.
Conclusion/significance: Tooth extraction but not endodontic treatment induces significant astroglial plasticity in the motor cortex. Astroglia may be a therapeutic target for preventing/curing postoperative sensory-motor impairments.

Overview

Many patients who undergo tooth extraction and endodontic treatments suffer from orofacial sensory (e.g., pain) and/or motor (e.g., jaw movement, biting, chewing) impairments, that can last for few days or months (Klineberg et al., 2014; Kumar et al., 2018; Donald R. Nixdorf et al., 2010; Renton, 2011). Clinicians often fail to adequately manage these impairments and prevent the development of chronic impairments (e.g., phantom sensation or pain) because the underlying mechanisms are still poorly understood. Current literature has shown in animals that clinically- or experimentally-induced acute orofacial pain may result in neuroplastic changes in brain regions

involved in the generation and modulation of sensory-motor functions (K. Adachi et al., 2007; Awamleh et al., 2015; Yao & Sessle, 2018). Such neuroplastic changes may contribute to the restoration of sensory-motor functions (i.e., adaptive neuroplasticity), but neuroplasticity may also contribute to the development and maintenance of impaired sensory-motor behaviours including chronic pain (i.e., maladaptive neuroplasticity). The orofacial primary motor cortex (oM1) is the main brain region involved in the initiation and control of orofacial motor functions. It is important to emphasize that all these functions are not exclusively 'motor' because they rely on somatosensory inputs from the orofacial region (e.g., oral mucosa, teeth) providing somatosensory feedback and feedforward information that is crucial for modulating the orofacial motor functions. Novel data from our group has shown that intraoral manipulations in rodents, such as orthodontic treatment, tooth trimming or extraction, dental implant surgery and acute noxious stimulation of the dental pulp, can induce functional changes in the oM1 manifested as variations in neuronal activity and circuitry (i.e., functional neuroplasticity). For review see (Avivi-ArberMartin et al., 2011; Avivi-Arber & Sessle, 2018b; B. J. Sessle et al., 2013). We have also reported that these changes may involve and depend on the functional integrity of non-neuronal glial cells since application of an astroglial inhibitor to the oM1 surface can reverse the neuroplasticity induced by the noxious stimulation of the dental pulp (Awamleh et al., 2015). However, while it is unclear what the exact cortical site of action of the astroglial inhibitor was in the cited study, it likely diffused into the cortex to exert its effects at least on astroglial cells within the superficial cortical layers. Changes in astroglial function are tightly coupled to changes in their number and/or morphology (S. Liddelow & Barres, 2015; Sun & Jakobs, 2012). In addition, it has been demonstrated that peripheral injuries (e.g., trauma to orofacial tissues or inflammation) result in activation of astroglial cells characterised by progressive changes in the number, morphology, function, and gene expression of astroglia (i.e., structural and functional astroglial plasticity), for review see (Chiang et al., 2012a; Alexei Verkhratsky & Butt, 2013). However, no study has addressed whether endodontic treatment (i.e., dental pulp extirpation) and tooth extraction induce astroglial plasticity in the orofacial primary motor cortex. Better understanding of the role and involvement of astroglia in orofacial motor functions after dental manipulation is of clinical significance since it can assist in the development of improved therapeutic approaches of orofacial sensory-motor impairment such as targeting astroglia within the orofacial primary motor cortex (Hamby & Sofroniew, 2010; Kimelberg & Nedergaard, 2010).

Conventional immunohistochemistry has long been a fundamental technique in neuroscience research to explore morphological features of neuronal and non-neuronal cell in consecutive thin brain sections. Major advancements in recent years have led to the development of the novel CLARITY technique that renders the brain optically transparent, and along with immunolabelling and subsequent novel 3D imaging and automated detection of brain cells allows for the quantification cellular morphological features in thick brain sections or even at the whole-brain level (Chung & Deisseroth, 2013a; Chung et al., 2013; H. Y. Zheng & Rinaman, 2016).

Thus, the general aim of the present thesis was to use an animal model and the CLARITY technique for 3D characterisation of the rat orofacial primary motor cortex and quantification of morphological changes in astroglial cells within thick brain sections of the orofacial primary motor cortex of rats receiving tooth extraction *versus* endodontic treatment.

All experimental procedures were approved by The University of Toronto Animal Care Committee, in accordance with the Canadian Council on Animal Care Guidelines and the regulations of The Ontario Animals for Research Act (R.S.O 1990). The experiments reported herein followed a strict standard protocol and all experimental procedures were carried out by the same investigator to ensure consistency and uniformity of the procedures. Data analysis was carried out in a blinded manner to reduce potential experimenter bias.

Materials and Methods

Animals

The present study was carried out on young adult male Sprague-Dawley rats (Charles River, Montreal, QC, Canada). Ras were 225-250 g upon arrival to the vivarium, and 300-340 g on the day of perfusion. All rats received a basic health assessment upon arrival (weight, skin, eyes, teeth and fur inspection). Consistent with our published (Limor Avivi-Arber et al., 2010; Avivi-ArberLee et al., 2015b) and ongoing studies, rats were single-housed (27 x 45 x 20 cm cages) to minimize social effects that might mask treatment outcome (Devor et al., 2007; Seminowicz et al., 2009). The cages contained a polyvinyl chloride tube (used as a shelter and a gnawing device) and were stored under the same temperature (21 ± 1 °C) and humidity (50 ± 5 %) controlled conditions and a 12-hour light/dark cycle (lights on at 07:00, off at 19:00 h). Consistent with our ongoing studies involving intraoral manipulations, all rats received mash chow diet and water *ad libitum* to avoid postoperative discomfort from biting on a hard diet and to ensure adequate food and drink intake. Consistent with the literature and our previous studies, since transportation and changes in husbandry environment are potentially stressful events that can significantly impact animals' health and function, which may in turn impact treatment effects on brain functions, all rats were subjected to a 7-day acclimation period (Fig. 7). Rats were monitored daily to assess body weight, food consumption and any change in their grooming, scratching or exploratory behavior.

Study design

A total number of four rats were used to optimise the CLARITY and immunofluorescence technique. A total number of 28 rats were used to test whether tooth extraction *versus* endodontic treatments can induce, one week later, differential changes in the morphological features of astroglial cells within the rat orofacial primary motor cortex. The one week time point was chosen since previous studies have shown that animals develop postoperative perioral hypersensitivity that peaks between postoperative day four and seven and thereafter subsides and returns to baseline within 14 days (Lakschevitz et al., 2011).

To prevent allocation bias, rats were randomly allocated into control and experimental groups (n=7/group). Rats of the extraction ('Exo') group received extraction of the three right maxillary molar teeth and rats of the endodontic ('Endo') group received endodontic treatment in the three right maxillary molar teeth. Rats of the 'Sham' group received the same general anaesthesia and mouth opening as the Exo and Endo groups but without actual tooth extraction or pulpectomy.

Rats of the 'Naïve' group received no treatment and no anaesthesia. Consistent with previous studies and to reduce postoperative pain and inflammation, rat received analgesics and anti-inflammatory drugs for the first three postoperative days. Rats were perfused on postoperative day seven (Fig. 6). Brains were extracted and thereafter 2 mm-thick coronal sections containing the orofacial motor cortex went through clearing and subsequent immunohistochemistry procedures to label astroglial cells as well as neurones. 3D imaging was carried out with a light sheet Z1 fluorescence microscope (Carl Zeiss, Jena, Germany) (20x CLARITY objective). Images were then processed with Bitplane Imaris software to automatically identify and quantify morphological features of astroglial processes.

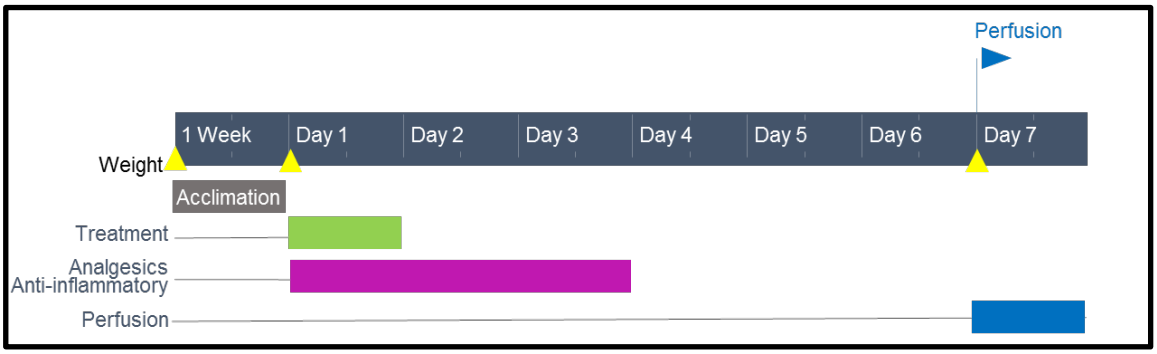

Figure 6. Experiment time-line. Rats were monitored on a daily basis from the date of arrival at the vivarium until perfusion day. Weight (yellow arrow) was measured on arrival, after acclimation period and on the day of perfusion. Treatment (endodontic treatment, or extraction, or sham operation) were carried out following a 1-week acclimation (green band). Analgesics and anti-inflammatory were administered up to three days post-op (pink band). Perfusion was performed on day 7 after treatment (blue band).

Animal experiments

All surgical procedures were carried out under standard aseptic surgical conditions with isoflurane/oxygen as a general anaesthesia (1-3% Isoflurane; 1L/min mixed with O_2) supplemented with local infiltration of lidocaine hydrochloride 0.1 ml, 2% in 1:100,000 epinephrine (Lignocaine, Lignospan standard®, Septodont, Ontario, Canada) injected to the labial and palatal sides of the three right maxillary molar teeth. Pulse oximeter monitoring verified that the heart rate and oxygen saturation levels were within a physiological range (i.e., 333–430 beats/min, 90-100% O_2). A controlled heating pad (Model 73A, YSI, Ohio, USA) maintained the rat core temperature at 37–37.5°C, and their eyes were treated with a lubricating ophthalmic ointment (Alcon®, Novartis, Canada). All the instruments used during the procedures were sterilized in an autoclave at 121°C .

Dental surgeries and sham operations were carried while the animal was under general anaesthesia (see above), lying in a supine position with a mouth being kept opened by pulling down the 2 mandibular incisors with a dental floss. The tongue was fixed to the left cheek with a tape (Fig. 7A). The surgical area was wiped using a cotton applicator soaked with 0.12% chlorhexidine gluconate (Peridex®, 3M ESPE, Canada), and a gauze was placed at the back of the throat to protect the rat from any aspiration. Thereafter, a local anaesthesic was injected into the palatal gingivae and buccal vestibule. All surgical procedures were carried out with the aid of an optical magnification of 4.5x using dental loupes (Orascoptic, Middleton, WI, USA).

Tooth extraction

The marginal gingiva around the three right maxillary molar teeth was gently detached. Then, the teeth were luxated using modified dental instruments (Avivi-ArberLee et al., 2015b; Avivi-Arber et al., 2017). Hemostasis was achieved by applying pressure to a sterile gauze pressed over the extraction sockets for a few minutes (Fig. 7C).

Endodontic treatment

Surface disinfection of the three maxillary molar teeth was carried out with 2.5 % sodium hypochlorite. The area was kept dry by continuous suctioning and application of a cotton roll to the buccal vestibule. For dental pulp extirpation, occlusal access cavities were drilled using a low-speed handpiece and a LN 25 carbide bur (Dentsply Maillefer, Ballaigues, Switzerland). Root canals were identified and cleaned using a filing motion with K-files #10; 21 mm long, bended at 2.5 mm from the tip, (Dentsply Maillefer, Ballaigues, Switzerland) and irrigated with 2.5% NaOCL with close and continuous suction (BabySmile S-502 Nasal Aspirator). When there was no more bleeding from the canals, a final irrigation with 2.5 % sodium hypochlorite for 1 minute per tooth was performed (Fig. 7D). Canals were dried with paper points and the pulp chamber was filled with an aqueous paste of calcium hydroxide (Vista Dental Products, Racine, WI, USA). The access cavity was sealed with IRM dental filling (Dentsply Maillefer, Ballaigues, Switzerland).

Sham Operation

Sham rats had exactly the same surgical operation as rats of the Exo and Endo groups including general and local anaesthesia, analgesics and anti-inflammatory drugs, and mouth opening for 30-60 min, and kept for a similar period of time that was used for the pulpectomy and extraction procedures of the Exo and Endo groups. However, no actual tooth extraction or endodontic treatment was carried-out in Sham rats.

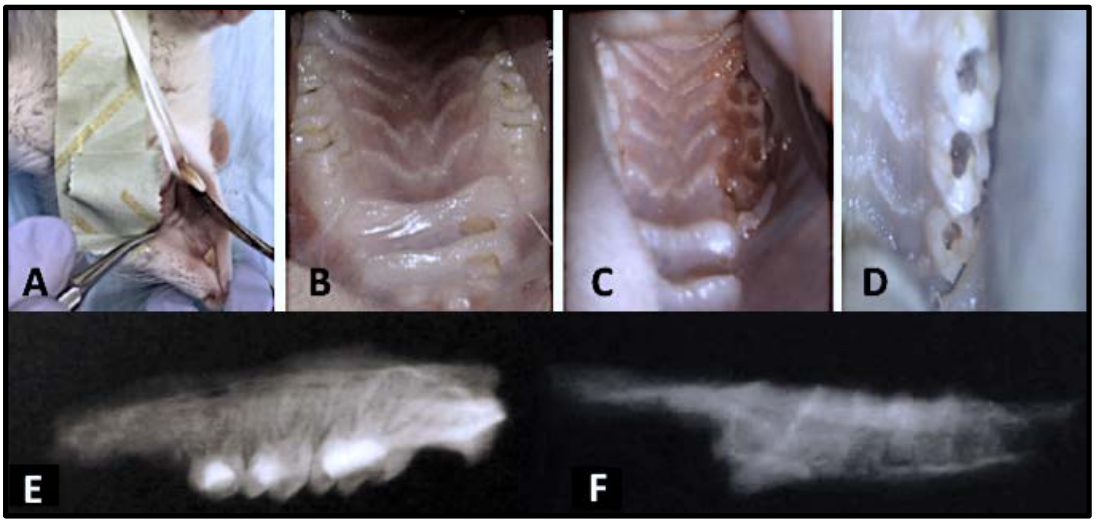

Figure 7. A. Mouth opening. **B.** Maxillary molar teeth. **C.** Extraction sockets of right maxillary molars. **D.** Access cavities for dental pulp extirpation of right maxillary molar teeth. **E.** Radiographic image of the right maxillae showing maxillary molar teeth after pulpectomy, restored temporarily. **F.** Radiographic image of the right maxillae showing extraction sockets.

Postoperative Care

After the surgical operation, rats were placed back into their cage under a heat lamp and monitored for 30 mins to ensure complete recovery from the general anaesthesia. Rats are known to develop periapical inflammatory changes after pupal extirpation (Holland, 1995). Whereas after tooth extraction they may develop postoperative perioral hypersensitivity that peaks between postoperative day 4 to 7 that thereafter subsides and returns to baseline within 14 days (Lakschevitz et al., 2011). Therefore, to reduce postoperative pain and inflammation following the surgical operations, buprenorphine hydrochloride (0.05 mg/kg, s.c., Buprenex, Reckitt Benckiser Healthcare Ltd, USA) and ketoprofen (5 mg/kg, .c., Anafen ® Injection, Boheringer Ingelheim, Canada) were administered subcutaneously every 8–12 h during the first three postoperative days. This postoperative care procedure was consistent with previous studies (Limor Avivi-Arber et al., 2010; Avivi-ArberLee et al., 2015b; Avivi-Arber et al., 2017). Consistent with previous studies, rats recovered uneventfully following the endodontic treatment (Erausquin & Muruzabal, 1967, 1968, 1969) and tooth extraction surgery (Avivi-ArberLee et al., 2015b). Following the operations, rats showed a normal feeding, grooming, scratching and exploratory behaviors, and a normal mean of daily rate of body weight gain.

Brain Tissue Clearing

All the procedures described below were adapted from the CLARITY Protocol developed by Karl Deisseroth's Lab at Stanford University (Deisseroth, 2017; Engberg, 2014). Some modifications

were introduced to optimise tissue clearing and immunolabelling of astroglial cells as well as neurones within the orofacial primary motor cortex, our region of interest.

Hydrogel Monomer Perfusion-Infusion and Embeding

General anaesthesia was induced with Ketamine HCl (175 mg/kg, Ketaset®, Ayerst Veterinary Laboratories, Ontario, Canada; I.M) and Xylazine (25 mg/kg, Rompun®, Bayer, Ontario, Canada). A deep state of anaesthesia was confirmed by the lack of a twitch in response to a strong pinch of the hindlimb. The rat was then placed on its back on the dissection pad in a supine position. A transverse incision was made with scissors first through the skin just below the ribs and then through the abdominal wall and ribs. Care was taken not to damage large blood vessels or organs such as the lungs and liver. The pericardium was gently detached from the heart. The anterior wall of the chest was raised and flipped backward to keep the heart exposed. A metal perfusion needle with a ball tip was inserted through the apex of the left ventricle into the aorta. When placed correctly, the tip of the perfusion needle was visible through the transparent wall of the aorta. The needle, just below the ball tip, was then secured to the aorta wall with a silk suture. Then, the right atrium was cut opened and 200 mL of ice-cold (4 °C) 1X PBS solution were perfused with a peristaltic pump (10 ml/min, ~5 - 10 min) through the needle and the right aorta to clear all blood from the capillaries in the brain and other body tissues. This step was followed by perfusion (10ml/min, ~5-10 min) of 200 ml of ice-cold fixative hydrogel solution (Fig. 8, Table 1). Adequate perfusion was confirmed by the appearance of a pale-color liver and a stiff tail (http://wiki.claritytechniques.org).

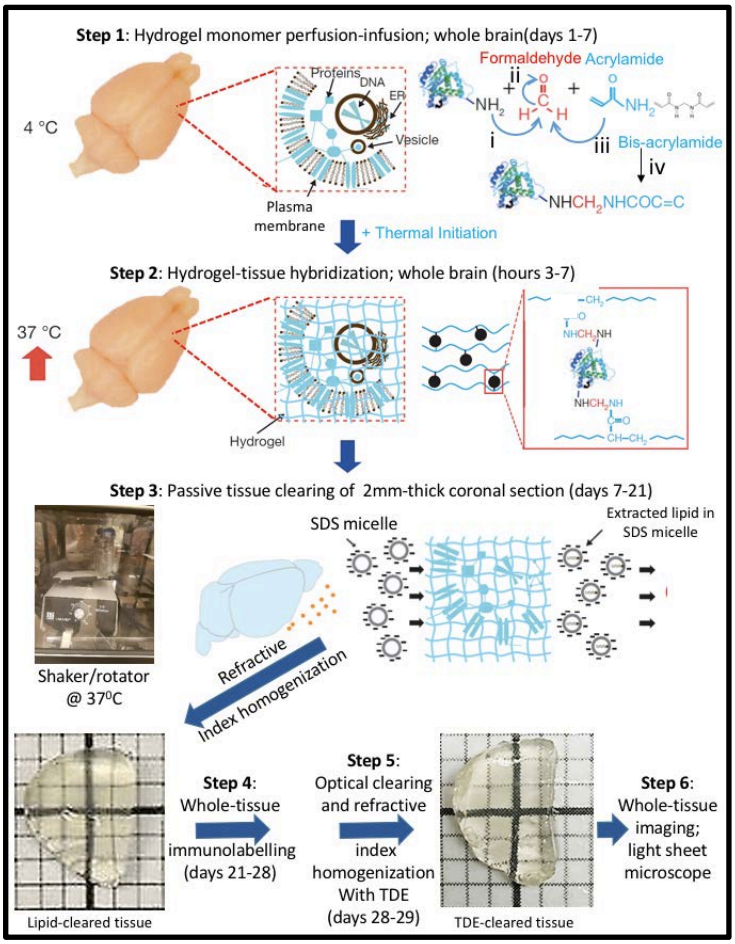

Figure 8. Overview CLARITY technique. Step 1: An optically transparent porous matrix composed of formaldehyde (red), acrylamide and bisacrylamide (hydrogel) monomers (blue), and thermally-triggered initiators, is perfusion-infused into the brain tissue at 40 ºC . The formaldehyde forms crosslinks with the tissue, and covalent links (electron sharing) between the hydrogel monomers and tissue-proteins, nucleic acids and other biomolecules. **Step 2:** At 37ºC, the tissue-bound monomers polymerize and create a hydrogel mesh–tissue hybrid that provides physical support to tissue structure. **Step 3:** Passive clearing removes lipids and molecules that remained unbound to the hydrogel. While detergent (sodium dodecyl sulfate, SDS) micelles diffuse passively through the tissue, they capture and clear out lipid of the tissue. The hydrogel–tissue hybrid keeps biomolecules and fine cytoarchitectural features of the brain intact, including neuronal and glial proteins. Despite clearing, some light-scattering remains due to heterogeneous distribution of proteins and nucleic acid complexes in the hybrid. **Step 4:** Standard immunolabelling of cells or molecules. **Step 5:** Immersion in 2,2'-thiodiethanol (TDE) solution for: optical clearing; tissue shrinkage to compensate for clearing-induced tissue expansion; refractive index homogenization. **Step 6:** Light sheet microscopy to visualise cells in intact thick tissue. Adapted by permission from Springer Nature: Nature Methods. CLARITY for mapping the nervous system, Kwanghun Chung, Karl Deisseroth, (2013).

Table 1 List of Solutions, ingredients and manufacturer.

Use/ Solution	Ingredients	Manufacturer
Perfusate		
Saline Solution. - 200 mL (1 rat)	1X PBS – 200 mL	Life Technologies
Fixative and substructure		
Hydrogel Solution. - 400 mL (2 rats)	Acrylamide (40% v/v) - 40 mL Bis-Acrylamide (2% v/v) - 10 mL Buffered Formalin Sol. 10% v/v - 100 mL VA-044 Initiator - 1 g (0.25 w/v) 10 X PBS - 40 ml Deionized water - 210 ml	Bio-Rad Bio-Rad EM Sciences WAKO BioShop
Storage		
Phosphate Buffered Saline Triton (PBST) 1 L (40 brains)	PBS 1X - 1L Triton-X 100 0.1% v/v - 1mL Sodium Azide - 0.1% w/v - 1 gr	Life Technologies BioShop Sigma
Clearing Buffer Solution - 10 L (56 brains)	Boric Acid - 123.66 g Deionized water - 2L Sodium hydroxide (NaOH) – adjust pH to 8.5 Sodium dodecyl sulfate (SDS) – 4% w/v-400mg Deionized water up to 10 L	BioShop BioShop Invitrogen
Buffer Wash		
Phosphate Borate Triton (PBT) - 1L (6 brains)	Boric acid - 12.5g Deionized water - 1L Sodium hydroxide (NaOH) – adjust pH to 8.5 Triton-X 100 0.1% - 1 mL Sodium Azide 0.1% w/v - 1 g	BioShop BioShop BioShop Sigma
Refractive Index Matching & Optical Clearing		
30% 2,2′-Thiodiethanol (TDE) - 100 mL (4 brains) 63 % TDE - 100 mL (4 brains)	TDE – 30 mL PBS 1X – 70 mL TDE 63 mL PBS 1X 7mL	Sigma Life Technologies Sigma Life Technologies

Brain Dissection

Immediately following the perfusion, the fixed brain was extracted from the skull. The skin, connective tissue and muscles surrounding the skull were cut and removed with scissors and a rongeur instrument, the first spinal vertebrae was cut out, the spinal cord was cut with the tip of fine scissors at the level of C2, then the rongeur was used to fracture the zygomatic arches, remove the auditory meatuses, and then to gently remove the skull from around the brain starting at the ventral surface of the skull, then going lateral and rostral. Then the brain was gently lifted to allow

for optical chiasm transection and trimming of any dura connecting the brain to the skull. Thereafter the olfactory nerves were transected, and the brain was gently lifted and removed out the skull. Special care was taken not to damage the motor cortical areas.

In addition, the rat maxillae were collected into 50 ml Falcon conical tubes containing 10 ml of 10% buffered formalin solution for radiographic evaluation of extraction sites and periapical tissue (Fig. 7 E, F).

Hydrogel Tissue Embedding

Each brain was placed in a 50 ml conical Falcon tube containing 25 mL of ice-cold hydrogel solution, and stored at 4 °C for 7 days to allow further diffusion of the hydrogel solution into the brain tissue.

Hydrogel-Tissue Hybridisation

The falcon tube with a loosened lid was placed in a desiccation chamber (in a fume hood) hooked up to a carbon dioxide tank and a vacuum pump (two falcon tubes at a time). A vacuum was applied to the chamber for 20 minutes to remove all oxygen (i.e., 'degassing') which was then replaced with inert 100% carbon dioxide gas flowing into the chamber for three minutes. Then, the falcon tube was quickly sealed to prevent reintroduction of oxygen. The tube was submerged in a temperature-controlled 37°C water-bath for 3-4 hours to polymerize and crosslink the hydrogel matrix.

After polymerization, the gel was peeled off from the brain with a lint-free tissue paper (KIMTECH Science®, Kimberly-Clark, Canada) and stored individually in a labelled 50 mL falcon tube with PBST solution until ready for sectioning. A mark was made to the right side of the brain to differentiate it from the left side. We used macroscopic anatomical features of the brain to determine the location of the orofacial primary motor cortex, corresponding to Swanson's atlas location ~2 – 4 mm anterior to Bregma (see Chapter 1 Fig. 2) (Swanson, 2004). The 2-millimeter thick coronal sections containing the orofacial primary motor cortex were cut with a vibratome 3000 (Model 3000, TPI, Missouri, USA). Each 2-mm thick section was stored in 50 ml Falcon tube with 25 ml of PSBT solution (Table 1) until ready for passive tissue clearing.

Passive clearing

Passive clearing of membrane lipids from each of the 2 mm-thick coronal section was carried-out by sequential immersions in a clearing solution (Table 1) within a 50 mL Falcon tube placed on a 3D Rotator platform (30 RPM, LAB-LINE) and incubated at 45°C. The section was first washed in 50 mL clearing solution for one day, and then for additional two days in fresh clearing solution to remove excess of formalin, initiator, and hydrogel monomers. Subsequently, 50 ml fresh clearing solution was changed every two days. The clearing was checked visually by holding the container up to the light until all lipids solubilized rendering the tissue completely transparent (i.e.,

'see-through' tissue) for microscopy (Engberg, 2014) (Fig. 9). Clearing took approximately 15 days.

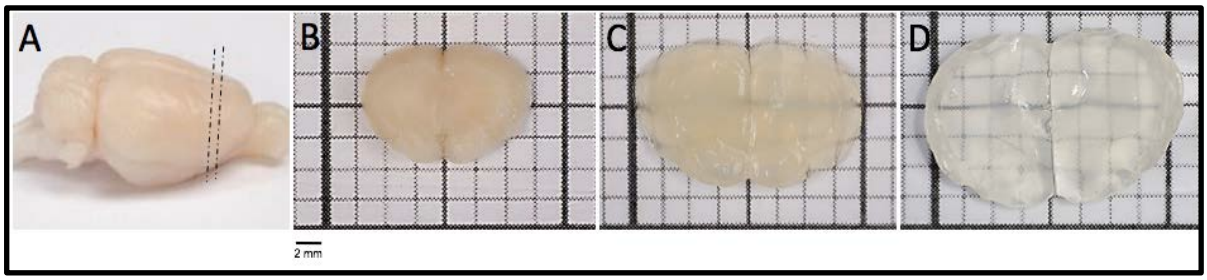

Figure 9. A. A whole brain after hybridisation (lined area) **B.** 2 mm-thick coronal section containing the motor cortex (rostral view) **C.** Coronal section after 7 days of passive clearing **D.** The tissue appeared 'see-through' after ~15 days of clearing. Notice the significant increase in size due to swelling that occurred during the passive clearing.

Following clearing, each section was placed in 50 mL buffer wash made of Phosphate Borate Triton (PBT) solution (Syed et al., 2017) (Table 1) in a falcon tube placed on a 3D rotator platform (30 RPM, LAB-LINE) at room temperature to wash out SDS micelles. The PBT was replaced three times per day for two days, and thereafter, the sections were stored in PBT solution at 4°C until tissue labelling.

Optimisation Protocol for Whole-Tissue Immunolabelling

The focus of this study was to introduce this method to our lab and optimise the immunolabelling of astroglial cells with a specific glial fibrillary acidic protein (GFAP) antibody to allow for subsequent characterisation and quantification of morphological features of astroglia within 2 mm-thick cleared motor cortex brain sections (Table 2) (Bastrup & Larsen, 2017; Bignami & Dahl, 1977; Chung & Deisseroth, 2013b; Chung et al., 2013; Costantini et al., 2015; Eng et al., 2000; Garcia-Cabezas et al., 2016; Tomer et al., 2014a) (http://wiki.claritytechniques.org/index.php/Immunostaining). In addition, we used and optimised immunolabelling of a neuronal nucleus marker (NeuN) that is known as Fox-3 protein, which is expressed exclusively by neurones and plays a role in regulating neuronal cell differentiation and nervous system development (Kim et al., 2009). NeuN is conventionally applied to distinguish astroglia from neurones and was used by us in this study to test whether an intraoral manipulation affected the number and size of neurones (Gusel'nikova & Korzhevskiy, 2015; Mullen et al., 1992).

We also used and optimised the immunolabelling with 4′,6-diamidino-2-phenylindole (DAPI), which is a blue-fluorescent DNA stain that is commonly used as a nuclear counterstain in fluorescence microscopy. DAPI has high affinity for DNA and has been use, for example, to count cells and sort them based on DNA content, or to measure cell apoptosis. We have used Alexa Fluor-conjugated antibodies as primary antibodies that are already directly conjugated to a fluorophore-coupled secondary antibody, thus eliminating the need for incubating the primary

antibody with a secondary antibody. This simplified and shortened the immunolabelling process since there was no secondary antibody incubation step, needing fewer washing steps. Conjugated antibodies are also cheaper. In addition, to save on material and incubation time, in the optimisation process we used 200 µm-thin coronal sections.

Whole-Tissue Immunolabelling Protocol

The 2 mm-thick sections were cut in the midline to separate the left and right hemispheres. Only the left hemispheres, contralateral to the dental manipulation side, were collected for immunolabelling since it has previously been documented that while orofacial muscles and tissues have bilateral representations within the orofacial motor cortex, the contralateral representations are significantly more predominant. Moreover, unilateral orofacial manipulations, such as tooth extraction, induce functional neuroplasticity mainly within the contralateral orofacial motor cortex (Kazunori Adachi et al., 2007; Limor Avivi-Arber et al., 2010; Avivi-ArberLee et al., 2015b).

Brain sections were transferred into new 50 ml Falcon tubes containing 0.5 mL PBST solution of 1:70 (7.1µl) anti-GFAP antibody conjugated to Alexa Fluor® 488, anti-NeuN antibody conjugated to Alexa Fluor® 555 and DAPI (Table 2). Tubes were placed on a rotating platform (at 30 RPM) and incubated at 37 °C for 6 days. Tissue sections were then washed in PBST at 37 °C for 6 days, changing PBST twice during working hours (i.e., 9 am and 6 pm). From this stage forward, the Falcon tubes were tightly covered with aluminum foil to protect the fluorescence antibodies from light and prevent fading (photobleaching) of the fluorophores.

Antibodies come in small amounts within small vials that were centrifuged before aliquoting to ensure all the material was at the bottom of the vial available for use.

Table 2 List of conjugated antibodies used for immunolabelling.

Antibody	Target	Manufacture	Catalog number	Wavelength Excitation (nm)	Wavelength Emission (nm)	Concentration/ 500µL PBST
Anti-Glial Fibrillary Acidic Protein (GFAP) Alexa Fluor® 488 Conjugate	Astroglial filaments	Sigma	MAB3402X	493 (Green)	519 (Green)	1:70 7.1 µL
Anti-NeuN clone A60 Alexa Fluor® 555 Conjugate	Neuronal nuclei	Sigma	MAB377A5	555 (Red)	565 (Red)	1:70 7.1 µL
4,6-Diamidino-2-phenylindole dihydrochloride (DAPI)	Nucleic acid all cell nuclei	AAT Bioquest	17510 (AAT)	356 (Blue)	461 (Blue)	1:70 7.1 µL

Imaging

A transparent brain tissue immersed in a solution of the same refractive index as its internal refractive index will appear invisible. Thus, the refractive index of the brain section had to be equilibrated to that of the imaging immersion medium, which in turn had to be matched as closely as possible to the refractive index of the imaging objective (Richardson & Lichtman, 2015). The objectives of the light sheet (LS) Z1 fluorescence microscope (Carl Zeiss, Jena, Germany) have a refractive index 1.45 which is suitable for imaging cleared tissue at a high-resolution.

FocusClear is the recommended immersion solution in the original CLARITY protocol, and in particular for thick-tissue sections like a whole mouse brain. FocusClear has shown to provide the optimal optical transparency and maximum imaging depth(Tomer et al., 2014b). However, it is an extremely expensive solution ($180 USD/ 5 ml). Other more affordable solutions with a RI of ~1.45, such as glycerol 87% (Tomer et al., 2014b) and 63% 2,2′-thiodiethanol (TDE) (Costantini et al., 2015; K. H. R. Jensen & Berg, 2017), can also be used but only for imaging thin tissue sections (< 1- 2 mm thick) or for a small imaging depth (http://wiki.claritytechniques.org).
Thus, glycerol and TDE were tested in this study to obtain the best tissue transparency and maximum imaging depth. GFAP- and NeuN-labelled sections went through serial incubations in series of TDE or glycerol solutions (Table 3).

For glycerol, the sections were incubated in different concentrations of the solution incrementally. First, the brain section was placed in 50 mL 25% (vol/vol) glycerol in 1X PBS (Glycerol/PBS) and stored in a Falcon tube on a 3D rotating platform (30 RPM) at 37 °C for 1 day (~24 hrs). Then, the sample was transferred to a new falcon tube containing 50 mL 50% (vol/vol) glycerol in 1X PBS and stored at the same conditions as before. Lastly, the sample was transferred to a new falcon tube containing 87% (vol/vol) glycerol in 1X PBS and stored at the same conditions as before and imaging was performed the following day (http://wiki.claritytechniques.org/index.php/Solutions). With glycerol the sections remained visually cloudy and this resulted in less penetration depth and less image quality.

For TDE, the sample was immersed in 50 mL of 30% (vol/vol) TDE in 1X PBS (TDE/PBS) (pH 7.5) and stored in a Falcon tube placed on a 3D rotating platform (30 RPM) at 37 °C. The section remained in the 30% TDE until its internal region got saturated with TDE as evident by its sinking to the bottom of the tube (~1.5 hrs). Then, the section was immersed in 50 mL 63% (vol/vol) TDE in same conditions as before and until the section sunk to the bottom of the tube (~1.5 hrs). After immersion in TDE, the sections became completely transparent but acquired a yellow hue. Sections also shrunk in TDE which appears to compensate for the swelling occurring following tissue clearing (Costantini et al., 2015; Epp et al., 2015).

We found that TDE, as compared with glycerol, provided a simpler and faster procedure for refractive index matching and optical clearing, and it also allowed for acquiring images with a deeper penetration depth and a higher resolution. Therefore, 63% TDE was used as the immersion solution for this study.

To further minimize refractory index mismatch and subsequent optical errors such as spherical aberrations (https://photographylife.com/what-is-spherical-aberration), and to improve the image quality and penetration depth, before each brain imaging the refractive index of the immersion

solution (63% TDE) was checked with a refractometer to ensure it is within 1.45 ± 0.03 (Fig. 10).

Figure 10. Refractometer used for determination of the Refractive Index (RI) of the cleared tissue, verifying that the RI of the 63% TDE solution before imaging in the light sheet microscope is 1.45.

Table 3 Testing options for optical clearing and refractive index matching

Solutions	Volume	Concentration	Rotation	Temperature	Time
Glycerol/PBS	50 mL	25%	30 RPM	37 °C	24 hrs
Glycerol/PBS	50 mL	50%	30 RPM	37 °C	24 hrs
Glycerol/PBS	50 mL	87%	30 RPM	37 °C	24 hrs
TDE/ 1X PBS	50 mL	30%	30 RPM	37 °C	Until sunk to the bottom of the tube (~1.5 hrs)
TDE/ 1X PBS	50 mL	63%	30 RPM	37 °C	Until sunk to the bottom of the tube (~1.5 hrs)

A glass capillary was glued with super-glue to the caudal side of the coronal section at a brain region distant from the region of interest (i.e. orofacial primary motor cortex) and not within the centres of light emission planes and objective. The tip of the capillary was then mounted to the microscope holder and the brain section was suspended from above into 63% TDE-filled chamber. This chamber provided the brain section with a stable temperature environment throughout the imaging process which took about 1/2 hour. For imaging the region of interest in layer I, the cortical oM1 was imaged while the coronal slide was submerged into the mounting solution, facing its rostral aspect to the objective. Care was taken not to form air bubble in the chamber to avoid light scattering.

Imaging the Region of Interest

The region of interest was determined to be ~ 4 mm from the midline (depicted with a red line) and including the superficial layer I based on our electrophysiology studies (Avivi-ArberMartin et al., 2011; Avivi-Arber et al., 2017; Awamleh et al., 2015) and the anatomical atlas (Swanson, 2004) (Fig. 11).

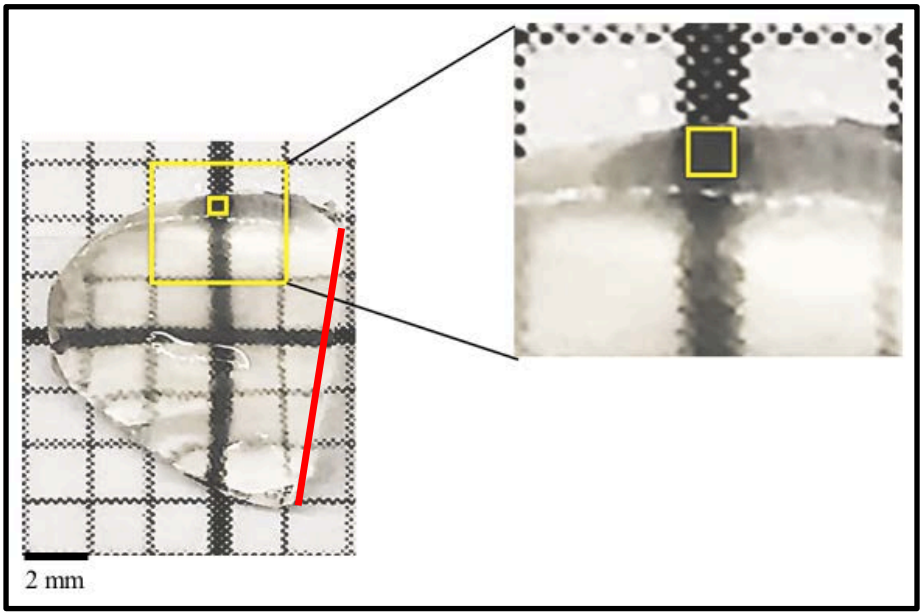

Figure 11. The region of interest is depicted in yellow was determined to be ~4 mm from the midline (red line) and included the superficial layer I. The total area scanned with the 20X CLARITY objective was 438.9 µm x 438.9 µm x 1 mm^3.

Imaging acquisition

A Zeiss light sheet Z1 microscope was used for image acquisition with the following specifications (Fig. 12):
Detection Optics: 20x/1.0 (CLARITY, RI=1.45)
Illumination Optics: 10x/0.2 x 2, 5x/0.1 x 2
Lasers: 405 nm (20mW), 488 nm (50 mW), 561 nm (20 mW), 638 nm (75 mW)
Camera: pCO Edge 5.5 x 2
Max Sample Dimensions: 10 x 10 x 20 (mm)
Field of View (20x): 439 x 439 (µm)
Software: Zeiss Zen Light sheet 2014
Environmental Control: Zeiss (temperature/CO_2)

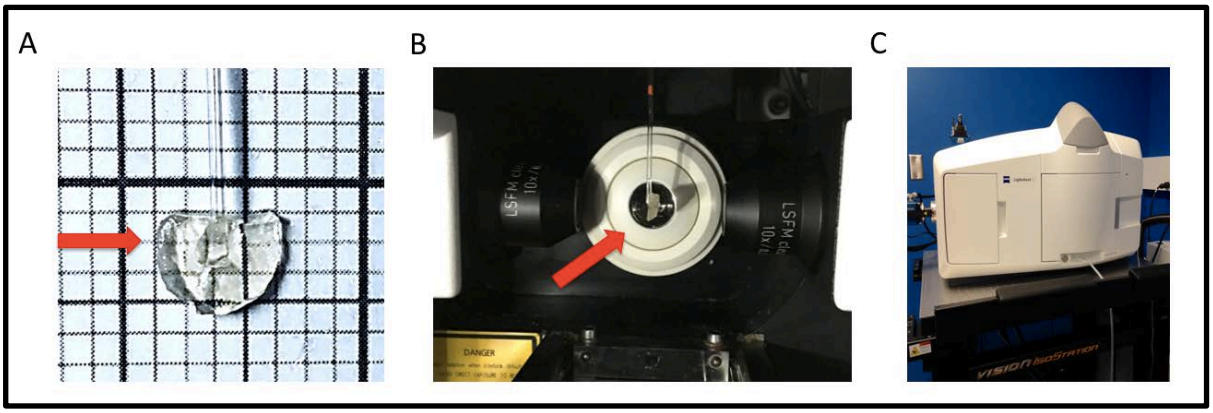

Figure 12. **A.** Red arrow is pointing at the area were the ROI is located. A glass capillary is attached to the caudal aspect of the thick brain section. **B.** The glass capillary with the brain section attached (red arrow) inside the Zeiss light sheet Z1 microscope. **C.** Outside view of the Zeiss light sheet Z1 microscope at the imaging facility.

Images of the region of interest were acquired with a CLARITY objective (Clr Plan-Neofluor 20x/1.0, RI=1.45 (± 0,03), NA=1. Acquisition parameters were as follow:

Unilateral illumination: Since usually only the left or right side illumination provided a better resolution image of the labelled neurones and astroglia, each plane was illuminated from either the left or right light source.

A separate track for each laser and camera color was used for each marker; GFAP (green 50), NeuN (red 50) and DAPI (cyan).

Laser power range: 45- 90%

Exposure time: 29 – 129 ms

Computers used for image acquisition require very large storage space as well a large random access memory (RAM) for image processing. The storage space of each acquired image of 2 mm-thick brain tissue was ~100 GB/scan. This storage volume was too large to be handled by the computers available at our imaging facility. Therefore, we carried out 2 scans of the region of interest which included 1 mm^3 of the rostral aspect of the region of interest, and then 1 mm^3 of the caudal aspect of the region of interest. We here report data collected from the rostral aspect only (i.e., ~60 GB/scan).

After imaging, the section was stored in PBST at room temperature protected from light.

Image processing

Image analysis was carried out with Imaris Software 9.2.0 (Bitplane) for 3D reconstruction. The Z- stacks acquired with the light sheet microscope Z1 were converted from Zen (.czi) files to Imaris (.ims) files using the Imaris File Converter x64 9.0.1 application. After background subtraction and thresholding for the green channel that corresponds to GFAP positive cells

(GFAP+), a systematic region of interest delineating Layer I was cropped from the total volume of the acquired image.

Cytoarchitectonic features were used to delineate the border between cortical layer I and layers II/III. Layers II/III, as compared with layer I, were characterised with a significantly larger number of NeuN positive (NeuN+) nuclei but only sparse GFAP immunoreactivity. In contrast, layer I was characterised by a rich network of GFAP+ processes and sparse NeuN immunoreactivity. The selected region of interest included layer I and excluded the glial limitans due to a significantly higher GFAP immunoreactivity of the glial limitans that limited the software ability to trace individual GFAP+ processes (Fig. 13).

Quantification of Morphological Features of Astroglial Processes

Accurate morphological description of filamentous structures requires ultimate resolution to capture the finest of structures of interest in our study, i.e., the astroglial processes. Therefore, the Filament Tracer application of Bitplane Imaris, an advanced software for automatic detection of filament-like structures, was used for morphometric analysis of astroglial processes in all spatial directions (Fig. 13 B and C).

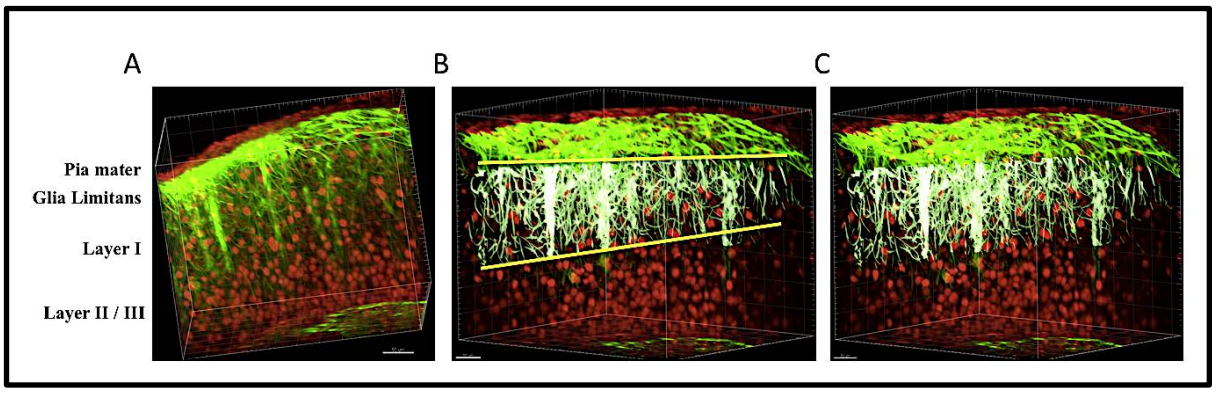

Figure 13. A. 3D image of 1 mm-thick cortical tissue showing the features used to select the region of interest within layer I: the pia mater, composed of NeuN+ flat-shape nuclei (red), the glia limitans identified as a continuous layer of high intensity GFAP+ astroglial cells, cortical layer I is characterised by a rich network of GFAP+ processes while layers II/III below show a significantly larger number of NeuN+ nuclei and sparse GFAP+ cells. **B.** Illustrate the region of interest within layer I selected for subsequent morphometric analysis of GFAP+ processes. Bottom yellow line marks the border between layer I and layers II/III. Top yellow line marks an approximate border between layer I and the glial limitans. **C.** Bitplane Imaris software masked the GFAP+ processes (selected in white) within the region of interest for subsequent morphometric analysis.

The tracing was done by applying the threshold based algorithm that is based on an absolute intensity threshold of GFAP+ filamentous structures (processes). Analysis took approximately 8 hours per scan.

Morphological parameters

Several statistic values were calculated automatically by the Imaris software and compiled in an Excel Sheet. For the purpose of our study, values from seven parameters were collected. The term 'Filament' is given by the software to the filamentous structures (astroglial processes) (http://www.bitplane.com/download/manuals/ReferenceManual6_1_0.pdf).

1. Filament Area: the sum of the generated surfaces of a frustum (truncated cone).
2. Filament Length (sum): the sum of the length of all filaments.
3. Filament mean diameter: the mean diameter within a filament. Each point of a filament line has its individual measured diameter. The diameter is measured as shortest distance from the Centre line to the surfaces defined by the lower threshold.
4. Filament volume: the sum of volume of all edges (cones) which compose a filament
5. Filament straightness: h = the distance between two branch points. The filament straightness is h per length of the filament.
6. Volume of layer I region of interest.
7. Changes in the complexity of astroglial morphology were determined by calculating the surface area/volume ratio from the data given by the software.

Data Analysis and Sample Size Calculation

The densely intermingled GFAP+ processes within layer I of the orofacial primary motor cortex did not allow analysis of morphological features of GFAP+ processes per individual cell. Therefore, data analysis was based on automatic software quantification of global morphological features of GFAP+ processes within the region of interest.

Our published and recent studies indicate large effect size (21-25%) between groups in primary outcomes. According to G*Power calculation, the minimum sample size required to obtain statistically significant results for ANOVA test with 80% power and a= 0.05 is n = 7/group, and for 4 groups a total of 28 rats. The outcome variables were transformed to obtain a normal distribution. The independent variable was the study group, i.e., Endo, Exo, Sham or Naive. The dependent variables were: sum of the total surface areas of all GFAP+ filaments, sum of the total length of all GFAP+ filaments, filaments' mean diameter, sum of the total volume of all GFAP+ filaments, mean filament straightness. The total volume (%), surface area, and length of GFAP+ filaments were normalised by the region of interest. Sigma Plot 11 (Systat Software, San Jose, CA, USA) was used to perform the statistical analysis. One-way ANOVA followed by the *post-hoc* Duncan test determined whether the independent variable had an effect on any of the independent

variables. A p-value < 0.05 was considered a statistically significant difference. Data are presented as means +/- SEM.

Excluded Data

A total of 32 rats were initially included in the study however, data of 10 rats were excluded because of animal death during the general anaesthesia (n=2), or inadequate perfusion (n=3) (Table 4). Inadequate perfusion was associated with bright wide-diameter (> 6 μm) GFAP+ structures consistent with blood-filled blood vessels (Fig. 14 A,B) (Whittington & Wray, 2017). Accordingly, for the mean diameter parameter, all the values larger than > 6 μm were not included for data analysis.

Additional 5 animals from the Naïve (n=3) and Exo (n=2) groups were excluded from the study due to inadequate quality of the images acquired with the light sheet microscope. Three images had bright/ dark stripe artifacts which are a common occurrence in light sheet microscopy (Power & Huisken, 2017) (Fig. 14 C,D). One Naïve rat was excluded due to a persistent technical problem with the statistical data extraction in the Imaris software. Thus, this study reports on a total of 22 rats with some groups having 5 rats.

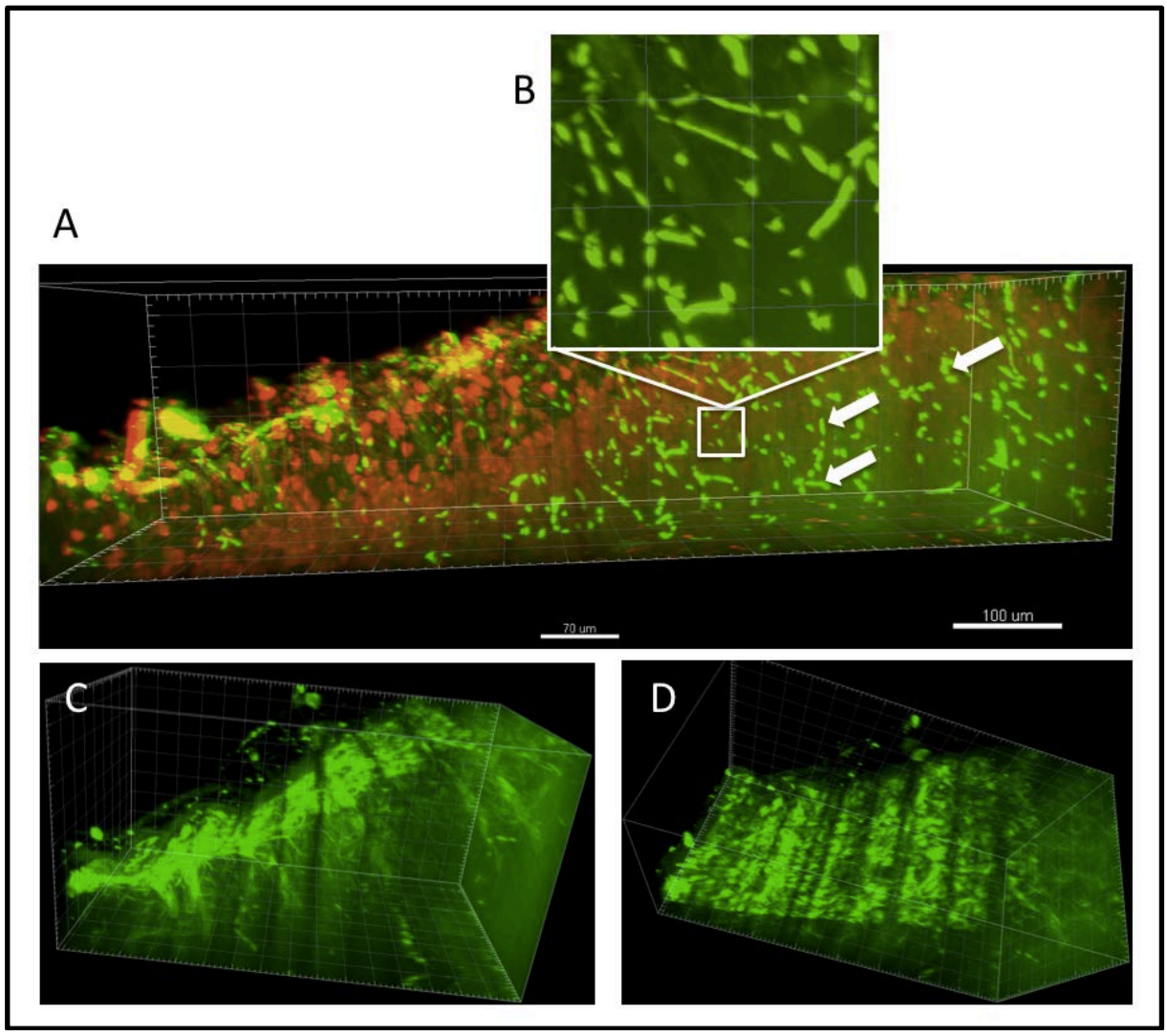

Figure 14. **A.** 3D image of 1 mm-thick brain tissue from a rat that underwent inadequate perfusion and subsequent immunolabelling with GFAP marker in green. White arrows show >6 µm-thick GFAP+ structures consistent with blood-filled blood vessels. **B.** Enlarged insert from figure **A. C and D.** 3D image of 1 mm-thick brain tissue which underwent immunolabelling with GFAP marker in green. Image shows bright and dark stripe artifacts which are a common occurrence in light sheet microscopy. **C.** A lateral view. **D.** A superior view.

Table 4 Summary of study groups, number of animals included or excluded from the study and the reason for exclusion.

Experimental Group	Number of Animals Included for analysis	Number of Animals Excluded	Reasons for exclusion
Naïve	**5**	**3**	- Two animals with bright/dark stripe artifacts - One animal with unsolved technical problem in statistical data extraction by Imaris software
Sham	**6**	**2**	- One animal with inadequate perfusion and bright blood-filled blood vessel artifacts - One animal died during general anaesthesia
Endo	**6**	**2**	- Two animals with inadequate perfusion and bright blood-filled blood vessel artifact
Exo	**5**	**3**	- Two animals with bright/dark stripe artifacts - One animal died during general anaesthesia
Total	**22**	**10**	

Results

In the present study we have utilised the CLARITY technique to render 2 mm-thick rat coronal brain sections optically transparent. We then utilised immunofluorescence labelling with antibody markers specific to astroglial filaments (GFAP) and neuronal nuclei (NeuN). We subsequently applied light sheet microscopy for 3D imaging of a motor cortex region we have previously defined as the centre of the rat orofacial primary motor cortex. By subsequently employing the Bitplane Imaris software for 3D reconstruction and morphometric analysis of the GFAP- and NeuN-labelled cells within the superficial layers I-III of the motor cortex we have identified their laminar distribution and have also characterised morphological features of astroglial processes within layer I of naïve rats and rats receiving tooth extraction, endodontic treatment or sham operation.

3D Characterisation of Astroglial and Neuronal Cytoarchitecture and Morphology within the Superficial Layers of the Rat Orofacial Primary Motor Cortex

We have identified a laminar cytoarchitecture of the primary motor cortex demonstrated by NeuN- and GFAP-immunoreactivity (i.e., NeuN+ and GFAP+, respectively). Fig. 15 C shows a 3D image of a 438.9 µm x 438.9 µm x 1 mm brain tissue from a representative rat immunolabelled with the NeuN and GFAP markers. The most superficial layer comprised a thin layer of NeuN+ flat-shape nuclei corresponding to the pia mater, i.e., the innermost layer of the meninges. The pia closely apposed a continuous layer of high-intensity GFAP+ cell bodies and processes, which are known as the glia limitans superficialis (glial limiting membrane) (also see Fig. 16). This membrane also surrounds the perivascular space surrounding the cortical parenchymal blood vessels and is referred to as the glia limitans perivascularis (Fig. 17). Immediately below the glia limitans is cortical layer I, which comprised a dense network of GFAP + cell bodies and processes, some of which project to the glia limitans. The immediately adjacent inner cortical layers, corresponding to cortical layers II/III, comprised an abundant number of NeuN+ round-shaped nuclei, significantly larger than the number of NeuN+ cells in layer I. In contrast, GFAP+ cells appear to be significantly more abundant in layer I than in layers II/III. DAPI was able to label (in blue) nuclei within the cortex and nuclei of the Pia mater located above the glia limitans (Fig. 16 D and Fig. 18 A).

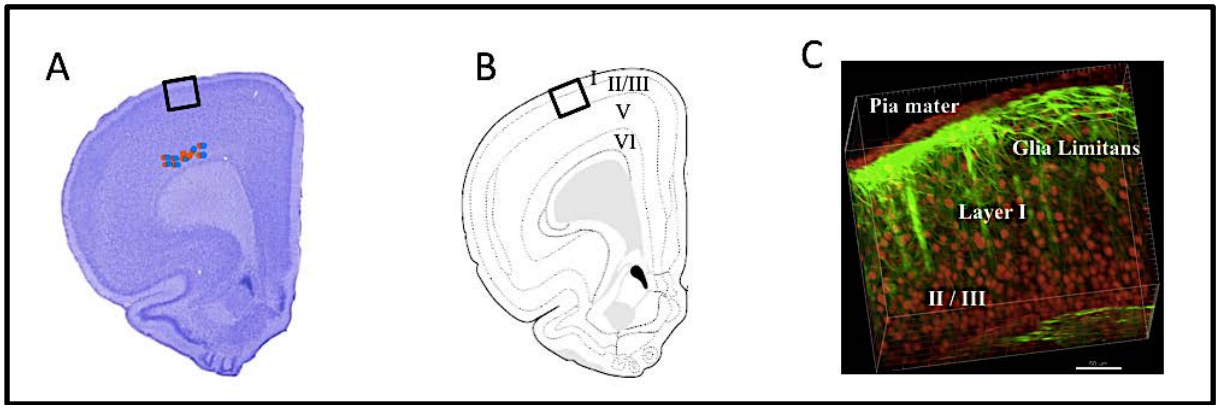

Figure 15. A. A 2D image of a Nissl-stained coronal section through the orofacial sensory-motor

cortex of a Sprague Dawley rat at ~ 3 mm anterior to Bregma. Superimposed are the jaw (red) and tongue (blue) motor representation areas as we have previously mapped and documented. **B.** A schematic diagram obtained from Swanson's Atlas of the Rat Brain). Reprinted with permission from John Wiley and Sons, Journal of Comparative Neurology, Brain maps 4.0—Structure of the rat brain: An open access atlas with global nervous system nomenclature ontology and flatmaps, Swanson L (2018) (Swanson, 2004), which corresponds to the histological section in **A,** indicating the different cortical layers numbered with Roman numerals from superficial to deep (I-VI). **C.** A 3D image of a 438.9 µm x 438.9 µm x 1 mm brain tissue showing the superficial cortical layers I and II/III as well as the pia mater and glia limitans. The pia is composed of NeuN+ flat-shape nuclei (red). Juxtaposing below the pia is the glia limitans, which comprises a continuous layer of high intensity GFAP+ astroglial cell bodies and processes. (GFAP+: immunoreactive glial fibrillary acidic protein; NeuN+: neuronal nuclei).

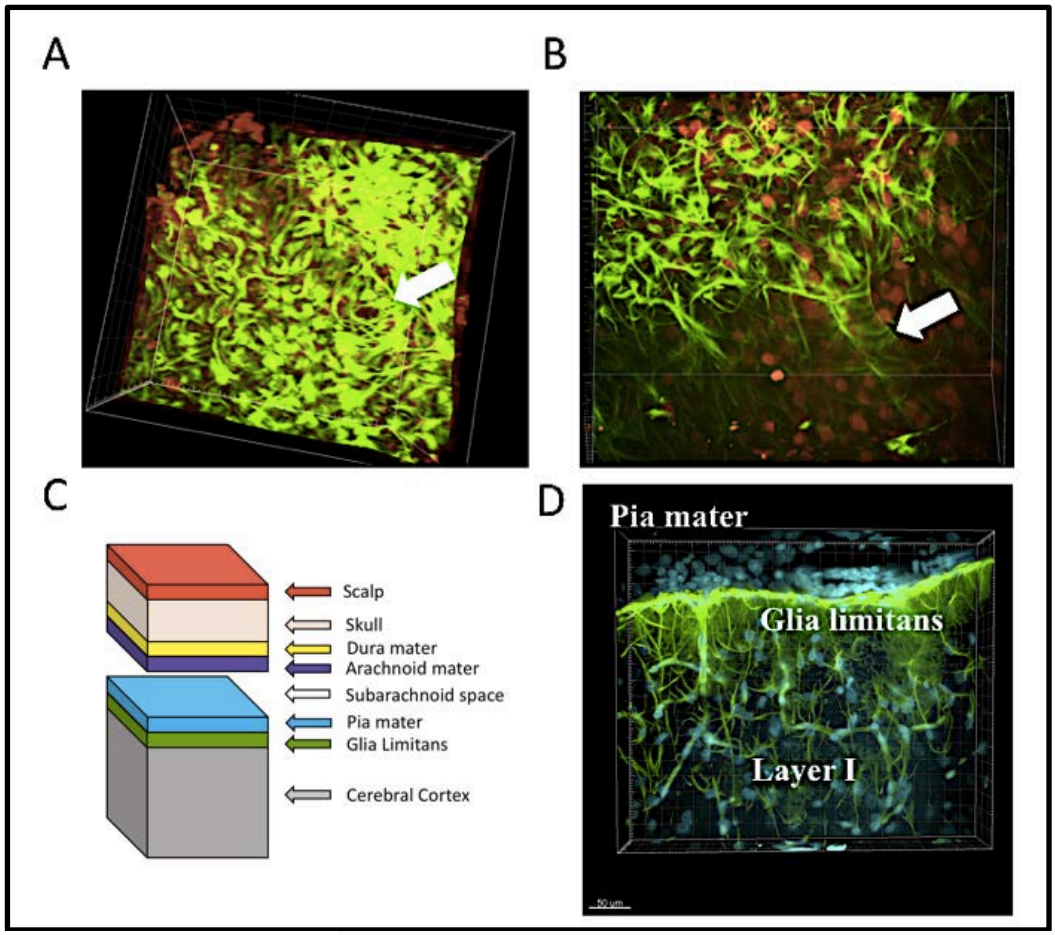

Figure 16. A. Superior view of glia limitans superficialis showing high-intensity GFAP+ cells (green) (soma and processes). Superior view of a blood vessel (white arrow) penetrating the cortex; and NeuN+ neuronal nuclei (red). **B.** Lateral view of a blood vessel (white arrow) penetrating the cortical parenchyma surrounded by GFAP+ astroglial cells (green) forming the glia limitans perivascularis; NeuN+ neuronal nuclei are marked in red. **C.** Schematic representation of the superficial membranes of the cortex showing that the glia limitans (green) lies between the pia mater and the cerebral cortex. **D.** 40 µm thick image showing GFAP + cells (green) within the superficial layer of motor cortex forming glia limitans, DAPI (blue) labelling of any nucleus within the cortex and the pia mater above the glia limitans.

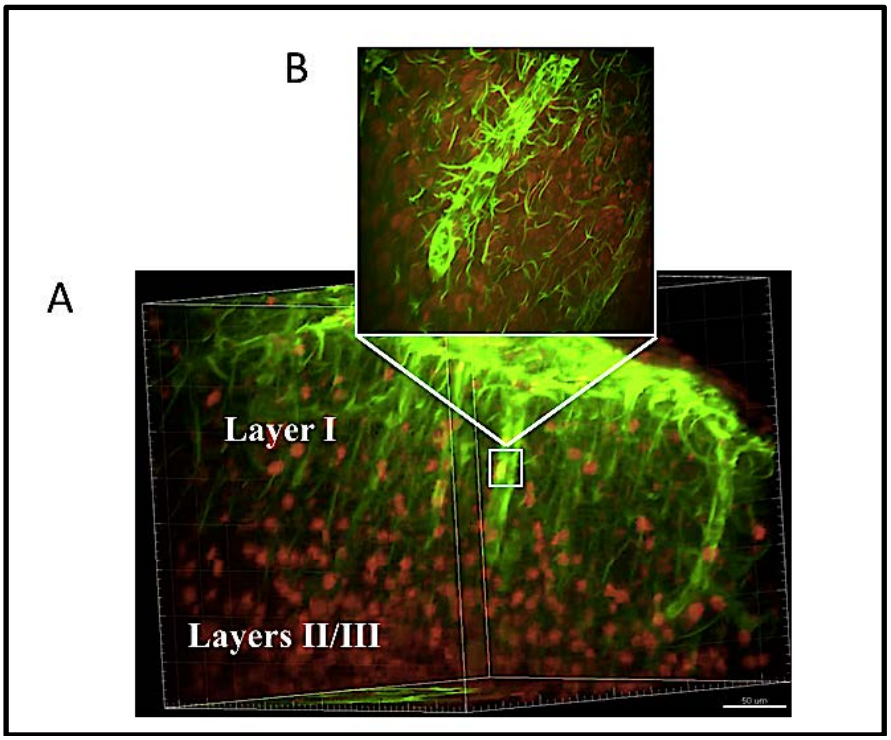

Figure 17. A. GFAP+ cells covering the cortical surface area form the glia limitans superficialis and GFAP+ cells surrounding blood vessels **B.** Enlarged insert from Figure A showing the glia limitans perivascularis.

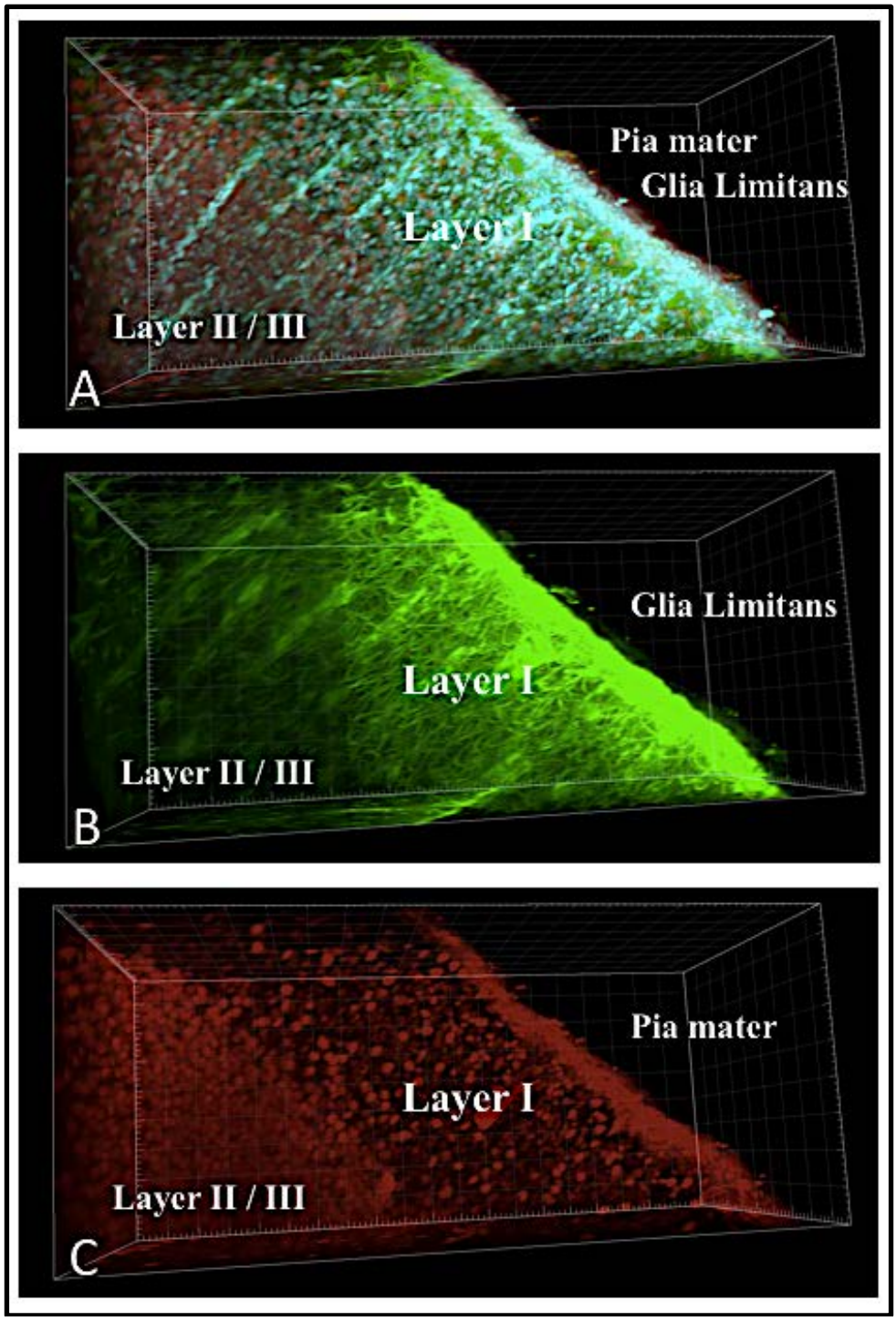

Figure 18. A. Shown superimposed are the three filtered fluorescent light channels that were used to visually isolate the marker used to label GFAP+ cells in green, NeuN+ cells in red, and non-selectively mark nuclei of any cell with DAPI+ in blue. **B.** Using here only the green channel, GFAP+ cells are highlighted. **C.** Using the red channel highlights only NeuN+ cells.

Morphological Features of GFAP-Immunoreactive Processes: Effects of Maxillary Molar Tooth Extraction *versus* Endodontic Treatment

Tooth extraction (Exo group), had a significant effect on the diameter of astroglial processes within the orofacial primary motor cortex. The mean diameter of astroglial processes of rats in the Exo group was significantly smaller than that of rats in the Naïve and Sham groups (ANOVA $F_{3,21}$=4.10 P= 0.022; *post hoc* Duncan's P=0.005, Sham: P= 0.028, respectively) and small, but not statistically significant, than that of rats in the Endo group. In contrast, the mean diameter of astroglial processes of rats of the Endo group was similar to that of rats in the Naïve and Sham groups (*post hoc* Duncan's P=0.148, 0.569, respectively), and was larger, but not statistically significant than that of rats in the Exo group (*post hoc* Duncan's p=0.066) (Fig. 19 A).
Tooth extraction, but not endodontic treatment, also had a significant effect on the straightness of astroglial processes. In comparison to Naïve and Sham groups, in the Exo group the astroglial processes were significantly straighter (ANOVA $F_{3,21}$=3.77 P= 0.030; *post hoc* Duncan's P=0.011, 0.032, respectively) (Fig. 19 B).

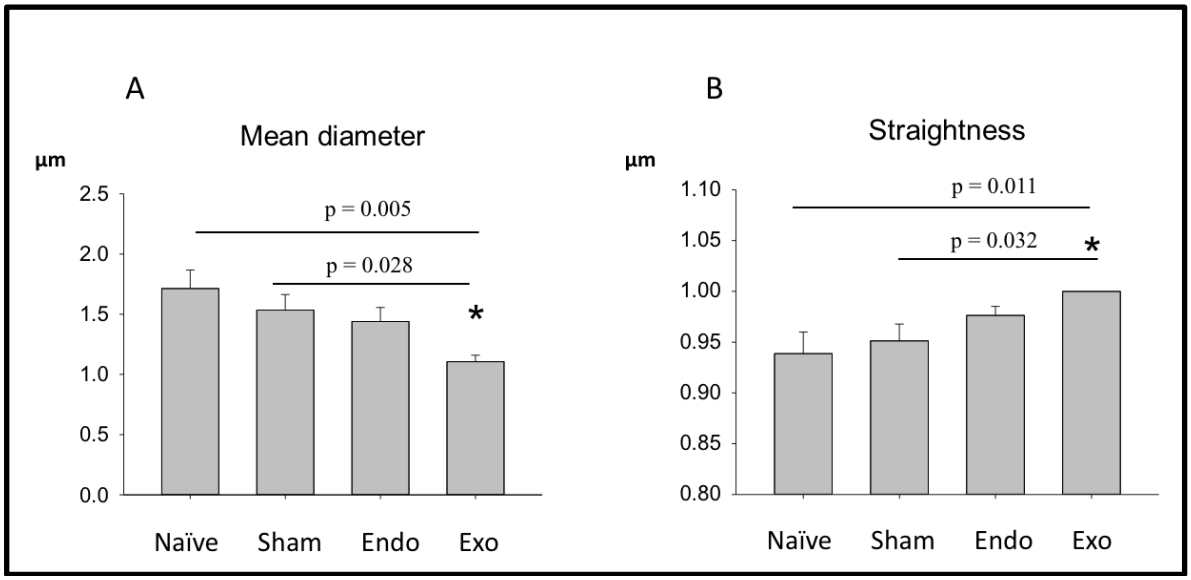

Figure 19. A. Mean diameter (**A**) and straightness (**B**) of astroglial processes. Tooth extraction was associated with a significantly smaller diameter and straighter astroglial processes.

No significant differences were found across the study groups in the volume, surface area to volume ratio, and length of astroglia processes (ANOVA, p > 0.050) (Fig. 20).

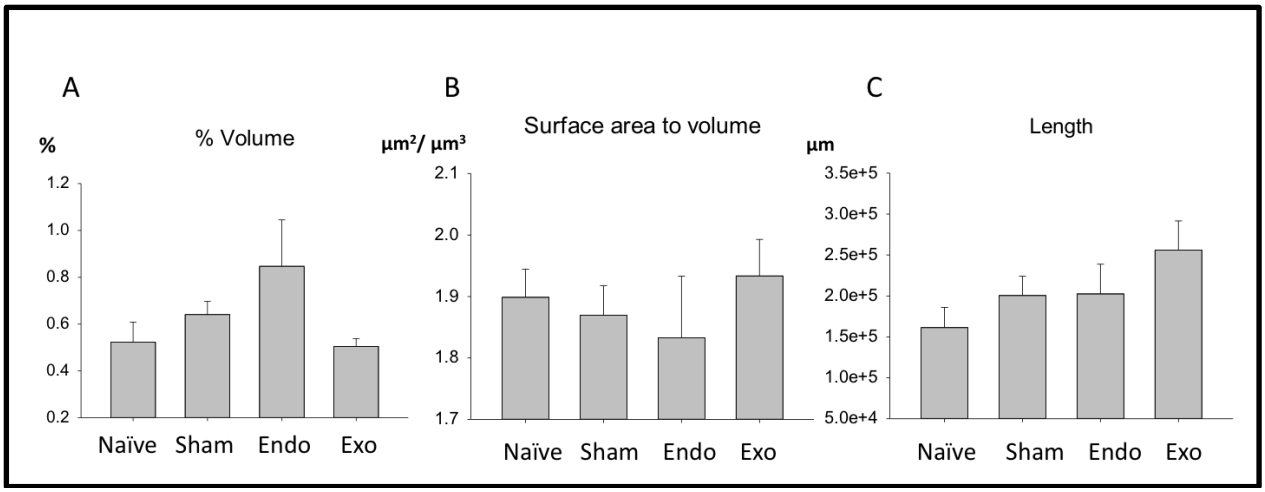

Figure 20. A. Percentage volume. **B.** Ratio surface area to volume. **C.** Length

Discussion

This study has successfully applied, for the first time, the novel **C**lear **L**ipid-exchanged **A**crylamide-hybridized **R**igid Imaging-compatible **T**issue-h**Y**drogel (**CLARITY**) technique to the orofacial primary motor cortex, rendering a 2 mm-thick section optically clear. With subsequent immunohistochemistry and the aid of light sheet microscopy we have successfully obtained, for the first time, large-volume high-resolution 3D images of a large block of cortex showing astroglia and neurones within the superficial layers (I-III) of a cortical region that we have previously identified as the centre of the orofacial primary motor cortex of adult male Sprague-Dawley rats. This study has also applied, for the first time, the Imaris software to automatically quantify morphological features of astroglial processes and test the effects of endodontic treatment *versus* tooth extraction on theses morphological features. Our novel findings suggest that tooth extraction has a statistically significant effect, one week later, on the morphological features of astroglial cells within the superficial layers of the rat orofacial primary motor cortex. Our results indicate that in comparison with Naïve rats and sham operated rats, tooth extraction is associated with thinner and straighter astroglial processes. On the other hand, endodontic treatment has no statistically significant effect on the morphological features of astroglial cells. The mean diameter and straightness of astroglial processes within the primary orofacial motor cortex of rats receiving endodontic treatment were similar to those in naïve rats and those in rats receiving sham operation. As discussed below, the differential effects of tooth extraction *versus* endodontic treatment on the morphological features of astroglia within the orofacial primary motor cortex may reflect differences in the rat sensory-motor function and functional adaptation (or maladaptation) to changes in orofacial sensory-motor functions induced by these treatments.

3D Visualisation of Astroglia with CLARITY

Astroglia communicate with each other and with neurones through an extensive network of processes that span within and through different regions and layers of the brain. Exploring their complex anatomy and connectivity requires 3D imaging of intact thick brain tissues. Conventional immunohistochemistry relies on a selective selection of a certain number of thin sections measured in a few μm up to several tens of μm out of a whole brain specimen. This unavoidably results in a loss of information and an inability to achieve 3D high-resolution images of complex cytoarchitecture that spans few millimeters or even centimeters within thick brain tissues or even the whole brain. Moreover, conventional immunohistochemistry is an irreversible process involving mounting of brain sections on slides. Thus, the slightest mistake in the process can ruin the whole sample or even a whole experiment. It also does not allow for re-staining or additional staining. The CLARITY technique, however, can overcome all these limitations of the conventional technique. CLARITY is based on the creation of a hydrogel scaffolding that stabilises the brain tissue and allows for membrane lipids to be removed without loss of the structural details and antigenicity of the tissues therein. This results in an intact, optically-transparent brain tissue that is permeable to large molecules and their chromophores including cellular antibodies for immunofluorescence labelling. It also facilitates 3D imaging of cells within a whole brain or thick tissue sections. In addition, there is no need for irreversible mounting, and the cleared tissue samples can be stored for months and go through multiple rounds of immunostaining with different fluorophores, which is particularly useful for multiplexing beyond the limits of spectral separation

(i.e., using multiple fluorophores that absorb and emit light in different parts of the visible spectrum in order to detect multiple molecules in a tissue) (Miller & Rothstein, 2016; Tomer et al., 2014a). In the present study we used and optimised immunostaining with Anti-GFAP, which is a standard and specific marker of astroglial filaments (Bastrup & Larsen, 2017; Bignami & Dahl, 1977; Chung & Deisseroth, 2013b; Costantini et al., 2015; Eng et al., 2000; Garcia-Cabezas et al., 2016; Tomer et al., 2014a), and Anti-NeuN, which is a standard and specific marker of neuronal nuclei (Gusel'nikova & Korzhevskiy, 2015; Kim et al.; Mullen et al., 1992). We also used DAPI, which is a blue-fluorescent stain of nuclear DNA in any cell. Thus, the present study has successfully applied for the first time the CLARITY technique to optically clear a 2 mm-thick sections of the orofacial primary motor cortex and has successfully optimised immunostaining of astroglial cells as well as neurones.

The novel light sheet microscope allows for high-speed and high-resolution 3D imaging of few millimeters- to a few centimeters-thick intact cleared tissues. Thus, the light sheet microscopy can exploit the CLARITY potential for 3D imaging of large populations of cells with complex cytoarchitecture spanning millimetres or even centimeters within an intact brain tissue (Dodt et al., 2007; Silvestri et al., 2015; Stefaniuk et al., 2016; Tomer et al., 2014a). However, these images generate an enormous amount of data that cannot be quantified manually. The Bitplane Imaris software can overcome this problem by allowing automatic identification and quantification of some morphological features of cells in the brain. Noteworthy is that the present study is the first to utilise the Imaris software for automatic identification and quantification of morphological features of astroglial processes in a large volume of brain tissue within the orofacial motor cortex layer I.

3D Characterisation of Astroglial and Neuronal Cytoarchitecture and Morphology within the Superficial Layers of the Rat Orofacial Primary Motor Cortex

This is the first study to provide large-volume (~0.5 x 0.5 x 1 mm^3) high-resolution 3D images of the highly organised laminar cytoarchitecture of the superficial layers of the orofacial primary motor cortex. Our findings are consistent with findings of published studies that have utilised conventional immunohistochemistry and histology. Of particular note is the abundance of neuronal nuclei within layers II/III and their sparse distribution in layer I. In contrast, the highly organized astroglial cells are sparse in layers II/III but abundant in layer I and form a dense network of processes, some of which project to the most superficial layer of the cortex known as the glia limitans superficialis (glial limiting membrane). Indeed, other studies have shown that in cortical layers II and III, the mean astroglia-to-neuron ratio is approximately 1:5 (Fleischhauer & Vossel, 1979; Kalman & Hajos, 1989; Takata & Hirase, 2008) and there is 1.6 times higher density of astroglial cells in layer I than in layers II and III (Takata & Hirase, 2008).

The finding of NeuN+ flat cells in the pia mater may correspond to a novel discovery. It has been published that meninges may serve as a source for delivery of neural precursors (Bifari et al., 2015; Nakagomi & Matsuyama, 2017); however, NeuN is not found in immature neural progenitor cells as long as they are not out of the cell cycle (Gusel'nikova & Korzhevskiy, 2015; Sarnat et al., 1998; Wolf et al., 1996). Moreover, the pia mater is a highly vascularized layer (Adeeb et al., 2013), therefore, the presence of NeuN+ cells in the pia mater might correspond to the vascular innervation of blood vessels (Pigolkin Yu et al., 1985). Interestingly, it is currently accepted that

small cerebral vessels and pia mater are insensitive to pain and that intracranial pain-sensitive structures are limited to the dura mater and its feeding pain (evidence is based on animal models) (Messlinger et al., 2008). However, this is inconsistent with recent observations from neurosurgeons while performing awake craniotomies in humans, suggesting that cerebral distal vessels and pia mater might actually be sensitive to mechanical stimuli and induce acute pain referred in the head (Fontaine & Almairac, 2017; Fontaine et al., 2018).

The glia limitans superficialis is a continuous layer composed of astroglial soma and a dense meshwork of astroglia processes that are firmly attached to an outer basal lamina that makes intimate contact with cells of the pia mater (Karasek, Swiltoslawski, and Zieliniska 2004, Liu et al. 2013). In addition, astroglial processes tightly ensheath the blood vessels that penetrate into the cortical parenchyma. This nearly-complete coverage of blood vessels through abundant astroglial endfeets is known as the 'glia limitans perivascularis'. The glia limitans superficialis is continuous with the glia limitans perivascularis and together they play a role in the control of the blood-brain barrier (BBB) (Quintana, 2017). In addition, the perivascular endfeet can release vasoactive substances that can mediate cerebral 'functional hyperemia', i.e., the increased or decreased cerebral blood flow associated with increased or decreased neuronal activity (Dunn & Nelson, 2014; MacVicar & Newman).

The finding of a rich network of astroglial cells within the superficial layers of the orofacial primary motor cortex supports previously published data (Awamleh et al., 2015) suggesting that superficial astroglial cells are involved in modulating motor cortex functional neuroplasticity (i.e., decreased excitability) induced by acute noxious stimulation of the dental pulp. This study has shown that application of an astroglial inhibitor to the surface of the orofacial primary motor cortex could reverse the neuroplasticity induced by the noxious stimulation (Awamleh et al., 2015). While it was unclear from the study what the exact cortical site of action of the astroglial inhibitor was, it likely diffused into the cortex to exert its effects, at least in part, on astroglial cells within the superficial cortical layers.

While the present study utilized the CLARITY immunohistochemistry in 2 mm-thick brain tissue to explore morphological features of marginal astroglial cells with layer I of the orofacial primary motor cortex, most of the available studies exploring astroglial structure and morphology have used mice and not rats as well as monkeys and human, and have characterised protoplasmic astroglia within layer II – VI of different cerebral cortical regions (Oberheim et al., 2009; Oberheim et al., 2008; Rodriguez et al., 2009; Sun et al., 2010; Wilhelmsson et al., 2004)(Miller & Rothstein). In addition, the majority of these studies have utilised the conventional immunohistochemistry technique using small (mm) and thin (40µm) brain sections which contain only few astroglial cells and used immunolabelling with different markers of astroglial cells (e.g., S-100, Glt, ALDA1L, GFAP), high-magnification (60x) imaging techniques and subsequent manual quantification of morphological features such as total diameter of the labeled astroglia, number of processes, the length of the processes, and the diameter of the soma or the thickest astroglial process. Therefore, we could not have made any comparison with published data. We have found that the mean diameter of astroglial processes within layer I ranged between 0.46 – 5.00 µm and the Mean $\pm$ SEM was 1.71 $\pm$ 0.15 µm. Oberheim et al found in mice that the thickest process measured 2.6 µm $\pm$ 0.2 µm (Oberheim et al., 2009).

In a recent published study, Miller and Rothstein (Miller & Rothstein, 2016) have utilised the CLARITY technique in transgenic mice expressing the astroglial proteins glutamate transporter (Glt1) and tdTomato-astros, and further immunolabelled with GFAP. By utilising single- and multi-photon microscopy to image 0.5- to 1.0 mm-thick brain tissue, they have characterised the laminar distribution of the different astroglial markers. However, they have not provided any details related to the cytoarchitecture and morphological features of the rich network of GFAP+ astroglial processes within the cortical layer 1.

Morphological Features of GFAP-Immunoreactive Processes: Effects of Maxillary Molar Tooth Extraction *versus* Endodontic Treatment

Tooth extraction, but not endodontic treatment, had a statistically significant effect on the morphological features of astroglial cells within the orofacial primary motor cortex. In comparison with naïve and sham-operated rats, in rats receiving tooth extraction, the astroglial processes were significantly finer (smaller mean diameter) and straighter, and they were also finer but not statistically significant than those in rats receiving endodontic treatment. There were no statistically significant differences between rats receiving endodontic treatment and those receiving sham operation or no treatment (i.e., the Naïve group).

The differences in the effects on cortical astroglial between tooth extraction and endodontic treatment may be related to differences in the extent of tissue injury, sensory denervation and the altered motor function. Following tooth extraction there is a major damage to hard and soft tissues as well as a complete loss of sensory inputs due to the lack of occlusal contacts and the loss of periodontal as well as pulpal tissues. In contrast, following endodontic treatment the amount of tissue injury is significantly smaller and there is also only a partial loss of occlusal contacts with no loss of periodontal ligament. Therefore, it is possible that the changes induced by the endodontic treatment were not significant enough to result in structural and morphological changes in astroglial processes, which is consistent with the notion that motor cortex plasticity emerges in response to significant changes external factors or experiences including changes in orofacial sensory-motor functions. However, these differences may also provide evidence that the orofacial primary motor cortex has the capability to adapt and be modelled in a task-dependent manner, but may also suggest the existence of different underlying mechanisms (Ebner, 2005; Haydon & Nedergaard, 2014; Monfils, 2005; Remple et al., 2001). It is also possible that the changes induced by endodontic treatment were too small to be detected by our methods or was within the range of normal variability and therefore could not be detected. It is important to consider that the analyzed data was underpowered and a large effect (21-25%) was contemplated for this study (see below study limitations). Another possibility relates to the reliability of our combined methods (light sheet microscope 20x objective and Imaris software) to accurately image astroglial processes and identify and delineate their boundaries for subsequent analysis of morphological features.

Similar study limitations to those described above may also account for our findings that neither tooth extraction nor endodontic treatment had any significant effect on any of the other measured variables, including volume (%), surface area (normalised), surface area to volume ratio and sum length of astroglial processes.

Our findings of decreased dimensions of astroglial processes are consistent with a couple of previously published studies. In a structural magnetic resonance study in rodents, molar tooth extraction was associated with a significantly decreased volume of the orofacial primary motor cortex region as well as other cortical regions involved in processing sensory and motor functions (Avivi-Arber et al., 2017). Our findings are also consistent with electrophysiological studies showing that molar tooth extraction is associated with decreased jaw and tongue motor representations in the orofacial primary motor cortex (Avivi-ArberLee et al., 2015b).

To our best knowledge, no other study has utilized the CLARITY immunohistochemistry to test the effects of intraoral injury on the morphological features of astroglia within the most superficial layer 1 of the orofacial primary motor cortex. Nevertheless, the findings of the present study appear to be in contradiction to the study by Laskawi et al., who have used conventional immunohistochemistry in rats who underwent transection of the facial motor nerve that supplies motor innervation to the facial muscles and vibrissae. The facial nerve transection was associated with increased immunoreactivity of various astroglial antigens in layers I/II and III/V of the primary motor cortex including S-100 protein which is a Ca2+-binding protein located mainly in the astroglial cytosol; GFAP which is a cytoskeletal filament protein, as well as connexin 43 which is a gap junction protein. The increased immunoreactivity occurred within 1 hour following the nerve transection and lasted for 2 to 5 days (Laskawi et al., 1997). The difference between their findings and ours may be due to the amount of peripheral injury, type of injured neural structure or the post-op time when these changes were sampled.

The findings of the present study of finer and straighter astroglial cells post-extraction also contradicted the notion that peripheral (e.g., nerve injury) and central (e.g., brain injury) injuries or neurological diseases (e.g., stroke), always induce astroglial reactivity that manifest in hypertrophy (i.e., reactive astroglia) within cortical (e.g., sensory and motor cortex) and subcortical (e.g., brainstem) brain regions. These hypertrophic changes manifest as upregulation of GFAP expression, increased volumes of soma and processes and increased immunoreactivity of astroglial antigens including GFAP. Nevertheless, such change depend on many factors including the type of injury and its severity, and brain region (Bernardinelli et al., 2014; Cheung et al., 2015; Childers et al., 2014; Genoud et al., 2006a; S. Liddelow & Barres, 2015; Miller & Rothstein, 2016; Oliet et al., 2001; Perez-Alvarez et al., 2014; Sun & Jakobs, 2012).

The contradicting findings reported in the present study as compared with those reported by other studies may be related to different study designs such as animal species, type and location of the injury, as well as the follow-up time since it has been documented that different brain mechanisms are involved at different points of time. It may also be related to the types of immunohistochemistry, imaging and data analysis techniques that were applied in the different studies.

Clinical Implications

It is now clear that astroglia not only provide metabolic support to neurones, but they also play an integral and even a crucial role in maintaining and partaking in neuronal synaptic activity. Astroglia release and remove neurotransmitters to and from the synaptic cleft, they can also

provide neurotrophic support and impact synapse formation and pruning and help maintain blood flow and blood-brain barrier. Significant to the present study, peripheral (e.g., nerve injury) and central (e.g., brain injury) injuries as well as neurological diseases (e.g., stroke), have been associated with astroglial plasticity manifested as changes in the structure and function of astroglial cells. Such changes can have a rapid or slow onset and last for a short duration and/or chronically and may subsequently enhance or impede recovery of sensory-motor functions following injury or disease (Bernardinelli et al., 2014; Cheung et al., 2015; Chung & Deisseroth, 2013b; Genoud et al., 2006b; S. A. Liddelow & Barres, 2017; Miller & Rothstein, 2016; Oliet et al., 2001; Perez-Alvarez et al., 2014). However, little is known of the involvement, role and underlying mechanisms of motor cortex astroglia in mediating neuronal response and sensory-motor behaviour to peripheral injury including following intraoral injury such as tooth extraction and/or pulpectomy. Nevertheless, this information is of clinical significance since patients receiving endodontic treatment or tooth extraction develop post-operative sensory-motor impairments such as pain and limited or altered jaw movement and altered biting forces. For reviews see (Avivi-ArberMartin et al., 2011; Avivi-Arber & Sessle, 2018a; B. Sessle et al., 2013; TrulssonVan der BiltCarlssonGotfredsenLarssonMueller et al., 2012) Moreover, in a significant number of patients these acute impairments may develop into a chronic sensory-motor conditions such as chronic orofacial pain, phantom bite or occlusal dysaesthesia (Hara et al., 2012; Kelleher et al., 2017; Marbach & Raphael, 2000; Melis & Zawawi, 2015; Nixdorf et al., 2012; Polycarpou et al., 2005b). For example, in 5-12% of the patients undergoing endodontic treatment and in 3% of the patient receiving tooth extraction, acute pain develops into a chronic pain condition (Donald R. Nixdorf et al., 2010; D. R. NixdorfE. J. Moana-Filho et al., 2010; Polycarpou et al., 2005a) Thus, a better understanding of the mechanisms underlying the development, maintenance and resolution of these conditions is crucial for the development of improved therapeutic strategies that target, for example, astroglial processes.

Study Limitations and Future Directions

The present study has successfully utilized the CLARITY immunohistochemistry technique in 1-2 mm-thick brain tissue in order to characterise cytoarchitecture and morphological features of astroglia and neurons within the superficial layers of the orofacial primary motor cortex, and to quantify the effects of tooth extraction *versus* endodontic treatment on these features.

The CLARITY immunohistochemistry is a multi-step technique that requires significant optimization and thus a large number of factors may affect the accuracy of the outcome. These include quality of the fluorescence images that can be affected by the adequacy of the animal perfusion, degassing the hydrogel solution to generate as little as possible air bubbles within the tissue, volumetric changes in the tissue after clearing, the quality and concentration of the antibodies and their ability to penetrate the full thickness of the brain section to achieve a high signal-to-background noise ratio and minimize nonspecific antibody binding. In the present study, although we have strictly adhered to the protocol for all brain samples, technical problems have precluded the inclusion of all animal samples in the final data analysis, which may have affected the statistical power by increasing the variance.

In general, statistical power is affected by the intervention effect size and the size of the sample used to detect effect of treatment. In the present study a large effect size (21-25%) was

estimated, based on our previously published studies. Due to the exclusion of some rats from all four groups, reducing the sample size to 6 or even 5 per group, it is possible the study did not have enough power to detect small changes induced by endodontic treatment. Moreover, it is also possible that the effect of endodontic treatment is smaller than the proposed effect size (i.e., lesser than 21-25%).

Expression of GFAP has become a prototypical marker for immunohistochemical identification of astroglial cells (Sofroniew & Vinters, 2010). It is also the oldest and most well-documented astroglial marker. GFAP is the key component responsible for assembly and extension of intermediate filaments inside the extended and thickened astroglial processes in astroglia reacting to injury (McKeon & Benarroch, 2018).

Another important limitation is that antibodies against GFAP label only the main processes of an astroglial cell that contains intermediate filaments, without labelling the full length of the main processes or its fine distal processes. In fact, GFAP delineates only approximately 15% to 20% of the total volume of astroglial cells in the cortex, leaving the true morphology undetected (Sun & Jakobs, 2012). Therefore, the method we used may have underestimated the effect of treatments on finer branches of the studied astroglia, and the pattern and 3D territory each cell occupies in naïve, sham and treated rats.

Another important limitation to consider is that the red blood cells naturally fluoresce across multiple wavelengths, expressing the emission and excitation spectra of many commonly used fluorescent reporters, including antibodies, dyes, stains, probes, and transgenic proteins, making it difficult to distinguish assay fluorescence from endogenous fluorescence (Whittington & Wray, 2017). In our study, we were able to identify > 6 μm-thick GFAP+ structures that were consistent with blood-filled blood vessels in animals that had incomplete ing transcardial perfusion. Such structures interfered with the immunofluorescent staining and complicated data analysis.

A drawback that results from using light sheet microscopy is the appearance of artifactual stripes that result from the unilateral illumination of the brain samples and the existence of optical obstacles (e.g., bubbles) that obscure the light sheet and result in light scattering and/or absorption. This typically leads to dark and bright stripes in the images impeding accurate morphometric analysis (see Chapter 2).

The use of only male rats precluded any assessment of possible sex differences that were documented in the sensory and motor effects of rats and humans to orofacial noxious stimuli (Cairns et al., 2001, 2002, 2003; Komiyama et al. 2005) and also in our preliminary data. Future studies could make use of both male and female rats to investigate possible sex differences in the effects of endodontic treatment and tooth extraction on the morphological features of astroglial cells within the orofacial primary motor cortex.

Future studies with a larger number of animals that would interrogate possible structural changes following oral treatment at different postoperative time points could unravel morphological features of astroglial at other cortical layers (e.g. Layers IV - VI) and thereby add further insights into differential time-dependent roles of astroglial cells in orofacial primary motor cortex changes after endodontic treatment and tooth extraction.

To date, astroglia are still misunderstood and unknown. Enabling scientists to obtain high-resolution volumetric imaging of thick clear tissue and the ability to quantify morphometric features, will likely yield groundbreaking findings that would improve our understanding of astroglial plasticity in health and disease.

Conclusions

Considering the crucial role that astroglia play in supporting and modulating neuronal activity in health and disease, and since injury and disease can induce rapid and chronic changes in astroglial structure and function which can either facilitate or impede sensory-motor recovery, developing novel methods to study astroglial structure is of paramount importance in neurophysiology research. Thus, our modified and optimised CLARITY immunohistochemistry technique along with our automatic Imaris software analysis protocol provide a novel tool to characterise astroglial morphology and plasticity in health and following injury or in disease.

Our novel findings of the laminar organisation of astroglia and neurones within the orofacial primary motor cortex and that tooth extraction, but not endodontic treatment, produces significant changes in morphological features of astroglial processes, facilitate pursuing future research directions to address the role of astroglia within the orofacial primary motor cortex in normal and pathological conditions. They also suggest that astroglia cells are a new and promising target for improved therapeutic interventions and prevention of impaired sensory-motor functions induced by injury or disease.

References

Adachi, K., Lee, J.-C., Hu, J. W., Yao, D., & Sessle, B. J. (2007). Motor cortex neuroplasticity associated with lingual nerve injury in rats. *Somatosens Mot Res, 24*(3), 97-109. doi:10.1080/08990220701470451

Adachi, K., Lee, J. C., Hu, J. W., Yao, D., & Sessle, B. J. (2007). Motor cortex neuroplasticity associated with lingual nerve injury in rats. *Somatosens Mot Res, 24*(3), 97-109. doi:10.1080/08990220701470451

Adeeb, N., Mortazavi, M. M., Deep, A., Griessenauer, C. J., Watanabe, K., Shoja, M. M., . . . Tubbs, R. S. (2013). The pia mater: a comprehensive review of literature. *Childs Nerv Syst, 29*(10), 1803-1810. doi:10.1007/s00381-013-2044-5

Adkins, D. L., Hsu, J. E., & Jones, T. A. (2008). Motor cortical stimulation promotes synaptic plasticity and behavioral improvements following sensorimotor cortex lesions. *Exp Neurol, 212*(1), 14-28. doi:10.1016/j.expneurol.2008.01.031

Al-Khateeb, T. H., & Alnahar, A. (2008). Pain experience after simple tooth extraction. *J Oral Maxillofac Surg, 66*(5), 911-917. doi:10.1016/j.joms.2007.12.008

Allen, N. J., & Barres, B. A. (2005). Signaling between glia and neurons: focus on synaptic plasticity. *Curr Opin Neurobiol, 15*(5), 542-548. doi:10.1016/j.conb.2005.08.006

Allen, N. J., & Barres, B. A. (2009). Glia — more than just brain glue. *Nature, 457*, 675. doi:10.1038/457675a

Araque, A. (2008). Astrocytes process synaptic information. *Neuron Glia Biol, 4*(1), 3-10. doi:10.1017/s1740925x09000064

Aroniadou, V. A., & Keller, A. (1993). The patterns and synaptic properties of horizontal intracortical connections in the rat motor cortex. *J Neurophysiol, 70*(4), 1553-1569. doi:10.1152/jn.1993.70.4.1553

Asanuma, H. (1989). *The Motor Cortex*. New York: Raven Press.

Avivi-Arber, L. (2009). *Face motor cortex neuroplasticity associated with alterations in the oral environment of the adult rat.* (Ph.D. Doctoral Thesis), University of Toronto, Toronto, Canada. Retrieved from http://hdl.handle.net/1807/19314

Avivi-Arber, L., Cherkas, P., Miyamoto, M., Varathan, V., Barashi-Gozal, M., Lakschevitz, F., . . . Sessle, B. J. (2010). Dental implant surgery is associated with nociceptive behaviour in rats. *13th World Congress on Pain, 10-A-3140-IASP*.

Avivi-Arber, L., Lakschevitz, F., Fung, M., Barashi-Gozal, M., Lee, J. C., Glogauer, M., & Sessle, B. J. (2011). Neuroplasticity of face sensorimotor cortex following dental extractions and implant surgery. *Society for Neuroscience Abstract Viewer and Itinerary Planner, 41*.

Avivi-Arber, L., Lee, J.-C., & Sessle, B. J. (2010). Effects of incisor extraction on jaw and tongue motor representations within face sensorimotor cortex of adult rats. *The Journal of Comparative Neurology, 518*(7), 1030-1045. doi:10.1002/cne.22261

Avivi-Arber, L., Lee, J.-C., & Sessle, B. J. (2011). Face sensorimotor cortex neuroplasticity associated with intraoral alterations. In J. P. Gossard, R. Dubuc, & A. Kolta (Eds.), *Breathe, Walk and Chew: The Neural Challenge: Part Ii* (Vol. 188, pp. 135-150).

Avivi-Arber, L., Lee, J. C., & Sessle, B. J. (2010). Cortical orofacial motor representation: Effect of diet consistency. *Journal of Dental Research, 89*(10), 1142-1147. doi:10.1177/0022034510373767

Avivi-Arber, L., Lee, J. C., & Sessle, B. J. (2011). Chapter 9--face sensorimotor cortex neuroplasticity associated with intraoral alterations. *Prog Brain Res, 188*, 135-150. doi:10.1016/b978-0-444-53825-3.00014-0

Avivi-Arber, L., Lee, J. C., & Sessle, B. J. (2015). Dental Occlusal Changes Induce Motor Cortex Neuroplasticity. *Journal of Dental Research, 94*(12), 1757-1764.

Avivi-Arber, L., Lee, J. C., Sood, M., Lakschevitz, F., Fung, M., Barashi-Gozal, M., . . . Sessle, B. J. (2015a). Long-term neuroplasticity of the face primary motor cortex and adjacent somatosensory cortex induced by tooth loss can be reversed following dental implant replacement in rats. *J Comp Neurol, 523*(16), 2372-2389. doi:10.1002/cne.23793

Avivi-Arber, L., Lee, J. C., Sood, M., Lakschevitz, F., Fung, M., Barashi-Gozal, M., . . . Sessle, B. J. (2015b). Long-term neuroplasticity of the face primary motor cortex and adjacent somatosensory cortex induced by tooth loss can be reversed following dental implant replacement in rats. *Journal of Comparative Neurology, 523*(16), 2372-2389. doi:10.1002/cne.23793

Avivi-Arber, L., Martin, R., Lee, J.-C., & Sessle, B. J. (2011). Face sensorimotor cortex and its neuroplasticity related to orofacial sensorimotor functions. *Archives of Oral Biology, 56*(12), 1440-1465. doi:10.1016/j.archoralbio.2011.04.005

Avivi-Arber, L., Martin, R., Lee, J. C., & Sessle, B. J. (2011). Face sensorimotor cortex and its neuroplasticity related to orofacial sensorimotor functions. *Arch Oral Biol, 56*(12), 1440-1465. doi:10.1016/j.archoralbio.2011.04.005

Avivi-Arber, L., Seltzer, Z., Friedel, M., Lerch, P. J., Moayedi, M., Davis, D. K., & Sessle, J. B. (2017). Widespread Volumetric Brain Changes following Tooth Lossin Female Mice. *Front Neuroanat, 10*, 121. doi:10.3389/fnana.2016.00121

Avivi-Arber, L., & Sessle, B. J. (2018a). Jaw sensorimotor control in healthy adults and effects of ageing. *J Oral Rehabil, 45*(1), 50-80. doi:10.1111/joor.12554

Avivi-Arber, L., & Sessle, B. J. (2018b). Jaw sensorimotor control in healthy adults and effects of ageing. *Journal of Oral Rehabilitation, 45*(1), 50-80. doi:10.1111/joor.12554

Awamleh, L., Pun, H., Lee, J. C., & Avivi-Arber, L. (2015). Decreased face primary motor cortex (face-M1) excitability induced by noxious stimulation of the rat molar tooth pulp is dependent on the functional integrity of face-M1 astrocytes. *Exp Brain Res, 233*(4), 1261-1272. doi:10.1007/s00221-015-4198-8

Bastrup, J., & Larsen, P. H. (2017). Optimized CLARITY technique detects reduced parvalbumin density in a genetic model of schizophrenia. *J Neurosci Methods, 283*, 23-32. doi:10.1016/j.jneumeth.2017.03.011

Ben Achour, S., & Pascual, O. (2012). Astrocyte-neuron communication: functional consequences. *Neurochem Res, 37*(11), 2464-2473. doi:10.1007/s11064-012-0807-0

Bernardinelli, Y., Randall, J., Janett, E., Nikonenko, I., Konig, S., Jones, E. V., . . . Muller, D. (2014). Activity-dependent structural plasticity of perisynaptic astrocytic domains promotes excitatory synapse stability. *Curr Biol, 24*(15), 1679-1688. doi:10.1016/j.cub.2014.06.025

Bifari, F., Berton, V., Pino, A., Kusalo, M., Malpeli, G., Di Chio, M., . . . Decimo, I. (2015). Meninges harbor cells expressing neural precursor markers during development and adulthood. *Front Cell Neurosci, 9*, 383. doi:10.3389/fncel.2015.00383

Bignami, A., & Dahl, D. (1977). Specificity of the glial fibrillary acidic protein for astroglia. *J Histochem Cytochem, 25*(6), 466-469. doi:10.1177/25.6.69656

Boroojerdi, B., Ziemann, U., Chen, R., Butefisch, C. M., & Cohen, L. G. (2001). Mechanisms underlying human motor system plasticity. *Muscle Nerve, 24*(5), 602-613.

Boudreau, S., Romaniello, A., Wang, K., Svensson, P., Sessle, B. J., & Arendt-Nielsen, L. (2007). The effects of intra-oral pain on motor cortex neuroplasticity associated with short-term novel tongue-protrusion training in humans. *Pain, 132*(1-2), 169-178. doi:10.1016/j.pain.2007.07.019

Bradl, M., & Lassmann, H. (2010). Oligodendrocytes: biology and pathology. *Acta Neuropathol, 119*(1), 37-53. doi:10.1007/s00401-009-0601-5

Brown, J. A. (2006). Recovery of motor function after stroke. In A. R. Moller (Ed.), *Reprogramming the Brain* (Vol. 157, pp. 223-228).

Buonomano, D. V., & Merzenich, M. M. (1998). Cortical plasticity: from synapses to maps. *Annu. Rev. Neurosci., 21*, 149-186.

Burish, M. J., Stepniewska, I., & Kaas, J. H. (2008). Microstimulation and architectonics of frontoparietal cortex in common marmosets (Callithrix jacchus). *J Comp Neurol, 507*(2), 1151-1168. doi:10.1002/cne.21596

Bushong, E. A., Martone, M. E., & Ellisman, M. H. (2004). Maturation of astrocyte morphology and the establishment of astrocyte domains during postnatal hippocampal development. *Int J Dev Neurosci, 22*(2), 73-86. doi:10.1016/j.ijdevneu.2003.12.008

Bushong, E. A., Martone, M. E., Jones, Y. Z., & Ellisman, M. H. (2002). Protoplasmic astrocytes in CA1 stratum radiatum occupy separate anatomical domains. *J Neurosci, 22*(1), 183-192.

Byers, M. R. (1984). Dental sensory receptors. *Int Rev Neurobiol, 25*, 39-94.

Chen, R. (2004). Interactions between inhibitory and excitatory circuits in the human motor cortex. *Exp Brain Res, 154*(1), 1-10. doi:10.1007/s00221-003-1684-1

Cheung, G., Sibille, J., Zapata, J., & Rouach, N. (2015). Activity-Dependent Plasticity of Astroglial Potassium and Glutamate Clearance. *Neural Plast, 2015*, 109106. doi:10.1155/2015/109106

Chiang, C. Y., Sessle, B. J., & Dostrovsky, J. O. (2012a). Role of Astrocytes in Pain. *Neurochemical Research, 37*(11), 2419-2431. doi:10.1007/s11064-012-0801-6

Chiang, C. Y., Sessle, B. J., & Dostrovsky, J. O. (2012b). Role of astrocytes in pain. *Neurochem Res, 37*(11), 2419-2431. doi:10.1007/s11064-012-0801-6

Chiang, C. Y., Wang, J., Xie, Y. F., Zhang, S., Hu, J. W., Dostrovsky, J. O., & Sessle, B. J. (2007). Astroglial glutamate-glutamine shuttle is involved in central sensitization of nociceptive neurons in rat medullary dorsal horn. *J Neurosci, 27*(34), 9068-9076. doi:10.1523/jneurosci.2260-07.2007

Childers, W. L., Prilutsky, B. I., & Gregor, R. J. (2014). Motor adaptation to prosthetic cycling in people with trans-tibial amputation. *Journal of Biomechanics, 47*(10), 2306-2313. doi:10.1016/j.jbiomech.2014.04.037

Chung, K., & Deisseroth, K. (2013a). CLARITY for mapping the nervous system. *Nature Methods, 10*(6), 508-513. doi:10.1038/nmeth.2481

Chung, K., & Deisseroth, K. (2013b). CLARITY for mapping the nervous system. *Nat Methods, 10*(6), 508-513. doi:10.1038/nmeth.2481

Chung, K., Wallace, J., Kim, S. Y., Kalyanasundaram, S., Andalman, A. S., Davidson, T. J., . . . Deisseroth, K. (2013). Structural and molecular interrogation of intact biological systems. *Nature, 497*(7449), 332-337. doi:10.1038/nature12107

Costantini, I., Ghobril, J. P., Di Giovanna, A. P., Allegra Mascaro, A. L., Silvestri, L., Mullenbroich, M. C., . . . Pavone, F. S. (2015). A versatile clearing agent for multi-modal brain imaging. *Sci Rep, 5*, 9808. doi:10.1038/srep09808

Dallerac, G., Chever, O., & Rouach, N. (2013). How do astrocytes shape synaptic transmission? Insights from electrophysiology. *Front Cell Neurosci, 7*, 159. doi:10.3389/fncel.2013.00159

DeFelipe, J., Alonso-Nanclares, L., & Arellano, J. I. (2002). Microstructure of the neocortex: comparative aspects. *J Neurocytol, 31*(3-5), 299-316.

Deisseroth, K. (2017). CLARITY Resources.

DeLuca, S., & Zarb, G. (2006). The effect of smoking on osseointegrated dental implants. Part II: Peri-implant bone loss. *International Journal of Prosthodontics, 19*(6), 560-566.

Devor, M., Gilad, A., Arbilly, M., Nissenbaum, J., Yakir, B., Raber, P., . . . Darvasi, A. (2007). Sex-specific variability and a 'cage effect' independently mask a neuropathic pain quantitative trait locus detected in a whole genome scan. *Eur J Neurosci, 26*(3), 681-688. doi:10.1111/j.1460-9568.2007.05704.x

Dodt, H. U., Leischner, U., Schierloh, A., Jahrling, N., Mauch, C. P., Deininger, K., . . . Becker, K. (2007). Ultramicroscopy: three-dimensional visualization of neuronal networks in the whole mouse brain. *Nat Methods, 4*(4), 331-336. doi:10.1038/nmeth1036

Donoghue, J., Wise SP. (1982). The motor cortex of the rat: cytoarchitecture and microstimulation mapping. *J Comp Neurol, 212*, 76-88.

Douglas, R. J., & Martin, K. A. (2004). Neuronal circuits of the neocortex. *Annu Rev Neurosci, 27*, 419-451. doi:10.1146/annurev.neuro.27.070203.144152

Dunn, K. M., & Nelson, M. T. (2014). Neurovascular signaling in the brain and the pathological consequences of hypertension. *Am J Physiol Heart Circ Physiol, 306*(1), H1-14. doi:10.1152/ajpheart.00364.2013

Ebner, F. F. (2005). *Neural plasticity in adult somatic sensory-motor systems*. Florida: CRS Press.

Eng, L. F., Ghirnikar, R. S., & Lee, Y. L. (2000). Glial fibrillary acidic protein: GFAP-thirty-one years (1969-2000). *Neurochem Res, 25*(9-10), 1439-1451.

Eng, L. F., Yu, A. C., & Lee, Y. L. (1992). Astrocytic response to injury. *Prog Brain Res, 94*, 353-365.

Engberg, K. (2014). CLARITY Protocol.

Epp, J. R., Niibori, Y., Hsiang, H. L., Mercaldo, V., Deisseroth, K., Josselyn, S. A., & Frankland, P. W. (2015). Optimization of CLARITY for Clearing Whole-Brain and Other Intact Organs. *eNeuro, 2*(3). doi:10.1523/eneuro.0022-15.2015

Erausquin, J., & Muruzabal, M. (1967). Root canal fillings with zinc oxide-eugenol cement in the rat molar. *Oral Surg Oral Med Oral Pathol, 24*(4), 547-558.

Erausquin, J., & Muruzabal, M. (1968). Tissue reaction to root canal cements in the rat molar. *Oral Surg Oral Med Oral Pathol, 26*(3), 360-373.

Erausquin, J., & Muruzabal, M. (1969). Tissue reaction to root canal fillings with absorbable pastes. *Oral Surg Oral Med Oral Pathol, 28*(4), 567-578.

Farkas, T., Perge, J., Kis, Z., Wolff, J. R., & Toldi, J. (2000). Facial nerve injury-induced disinhibition in the primary motor cortices of both hemispheres. *European Journal of Neuroscience, 12*(6), 2190-2194. doi:10.1046/j.1460-9568.2000.00096.x

Fleischhauer, K., & Vossel, A. (1979). Cell densities in the various layers of the rabbit's striate area. *Anat Embryol (Berl), 156*(3), 269-281.

Fontaine, D., & Almairac, F. (2017). Pain during awake craniotomy for brain tumor resection. Incidence, causes, consequences and management. *Neurochirurgie, 63*(3), 204-207. doi:10.1016/j.neuchi.2016.08.005

Fontaine, D., Almairac, F., Santucci, S., Fernandez, C., Dallel, R., Pallud, J., & Lanteri-Minet, M. (2018). Dural and pial pain-sensitive structures in humans: new inputs from awake craniotomies. *Brain, 141*(4), 1040-1048. doi:10.1093/brain/awy005

Fried K., G. J. L. (2014). *The Dental Pulp*. Berlin, Heidelberg: Springer.

Frost, S. B., Barbay, S., Friel, K. M., Plautz, E. J., & Nudo, R. J. (2003). Reorganization of remote cortical regions after ischemic brain injury: A potential substrate for stroke recovery. *J Neurophysiol, 89*(6), 3205-3214. doi:10.1152/jn.01143.2002

Garcia-Cabezas, M. A., John, Y. J., Barbas, H., & Zikopoulos, B. (2016). Distinction of Neurons, Glia and Endothelial Cells in the Cerebral Cortex: An Algorithm Based on Cytological Features. *Front Neuroanat, 10*, 107. doi:10.3389/fnana.2016.00107

Genoud, C., Quairiaux, C., Steiner, P., Hirling, H., Welker, E., & Knott, G. W. (2006a). Plasticity of astrocytic coverage and glutamate transporter expression in adult mouse cortex. *PLoS Biol, 4*(11), e343. doi:10.1371/journal.pbio.0040343

Genoud, C., Quairiaux, C., Steiner, P., Hirling, H., Welker, E., & Knott, G. W. (2006b). Plasticity of astrocytic coverage and glutamate transporter expression in adult mouse cortex. *Plos Biology, 4*(11), 2057-2064. doi:e343

10.1371/journal.pbio.0040343

Guggenmos, D. J., Barbay, S., Bethel-Brown, C., Nudo, R. J., & Stanford, J. A. (2009). Effects of tongue force training on orolingual motor cortical representation. *Behav Brain Res, 201*(1), 229-232. doi:10.1016/j.bbr.2009.02.020

Gundersen, V., Storm-Mathisen, J., & Bergersen, L. H. (2015). Neuroglial Transmission. *Physiol Rev, 95*(3), 695-726. doi:10.1152/physrev.00024.2014

Gusel'nikova, V. V., & Korzhevskiy, D. E. (2015). NeuN As a Neuronal Nuclear Antigen and Neuron Differentiation Marker. *Acta Naturae, 7*(2), 42-47.

Haggard, P., & de Boer, L. (2014). Oral somatosensory awareness. *Neurosci Biobehav Rev, 47*, 469-484. doi:10.1016/j.neubiorev.2014.09.015

Hamby, M. E., & Sofroniew, M. V. (2010). Reactive astrocytes as therapeutic targets for CNS disorders. *Neurotherapeutics, 7*(4), 494-506. doi:10.1016/j.nurt.2010.07.003

Hammond, C. (2008). *Cellular and Molecular Neurophysiology* (Elsevier Ed. Third Edition ed.).

Hara, E. S., Matsuka, Y., Minakuchi, H., Clark, G. T., & Kuboki, T. (2012). Occlusal dysesthesia: a qualitative systematic review of the epidemiology, aetiology and management. *J Oral Rehabil, 39*(8), 630-638. doi:10.1111/j.1365-2842.2012.02300.x

Hathway, G. J., Vega-Avelaira, D., Moss, A., Ingram, R., & Fitzgerald, M. (2009). Brief, low frequency stimulation of rat peripheral C-fibres evokes prolonged microglial-induced central sensitization in adults but not in neonates. *Pain, 144*(1-2), 110-118. doi:10.1016/j.pain.2009.03.022

Haydon, P. G., & Nedergaard, M. (2014). How do astrocytes participate in neural plasticity? *Cold Spring Harb Perspect Biol, 7*(3), a020438. doi:10.1101/cshperspect.a020438

Holland, G. R. (1995). Periapical neural changes after pulpectomy. *Oral Surg Oral Med Oral Pathol Oral Radiol Endod, 80*(6), 726-734.

Hossain, M. Z., Unno, S., Ando, H., Masuda, Y., & Kitagawa, J. (2017). Neuron-Glia Crosstalk and Neuropathic Pain: Involvement in the Modulation of Motor Activity in the Orofacial Region. *Int J Mol Sci, 18*(10). doi:10.3390/ijms18102051

Huntley, G. W. (1997). Differential effects of abnormal tactile experience on shaping representation patterns in developing and adult motor cortex. *Jouranl of Neuroscience, 17*(23), 9220-9232.

Iyengar, S., Qi, H. X., Jain, N., & Kaas, J. H. (2007). Cortical and thalamic connections of the representations of the teeth and tongue in somatosensory cortex of new world monkeys. *J Comp Neurol, 501*(1), 95-120. doi:10.1002/cne.21232

Jacobs, K. M., & Donoghue, J. P. (1991). RESHAPING THE CORTICAL MOTOR MAP BY UNMASKING LATENT INTRACORTICAL CONNECTIONS. *Science, 251*(4996), 944-947. doi:10.1126/science.2000496

Jensen, K. H., & Berg, R. W. (2016). CLARITY-compatible lipophilic dyes for electrode marking and neuronal tracing. *Sci Rep, 6*, 32674. doi:10.1038/srep32674

Jensen, K. H. R., & Berg, R. W. (2017). Advances and perspectives in tissue clearing using CLARITY. *J Chem Neuroanat, 86*, 19-34. doi:10.1016/j.jchemneu.2017.07.005

Kaas, J. H. (1991a). Plasticity of sensory and motor maps in adult mammals. *Annual Review of Neuroscience, 14*, 137-167.

Kaas, J. H. (1991b). Plasticity of sensory and motor maps in adult mammals. *Annu Rev Neurosci, 14*, 137-167. doi:10.1146/annurev.ne.14.030191.001033

Kaas, J. H., Qi, H. X., & Iyengar, S. (2006). Cortical network for representing the teeth and tongue in primates. *Anat Rec A Discov Mol Cell Evol Biol, 288*(2), 182-190. doi:10.1002/ar.a.20267

Kalman, M., & Hajos, F. (1989). Distribution of glial fibrillary acidic protein (GFAP)-immunoreactive astrocytes in the rat brain. I. Forebrain. *Exp Brain Res, 78*(1), 147-163.

Kelleher, M. G., Rasaratnam, L., & Djemal, S. (2017). The Paradoxes of Phantom Bite Syndrome or Occlusal Dysaesthesia ('Dysesthesia'). *Dent Update, 44*(1), 8-12, 15-20, 23-14, 26-18, 30-12. doi:10.12968/denu.2017.44.1.8

Kettenmann, H., & Verkhratsky, A. (2008). Neuroglia: the 150 years after. *Trends Neurosci, 31*(12), 653-659. doi:10.1016/j.tins.2008.09.003

Kim, K. K., Adelstein, R. S., & Kawamoto, S. (2009). Identification of neuronal nuclei (NeuN) as Fox-3, a new member of the Fox-1 gene family of splicing factors. *J Biol Chem, 284*(45), 31052-31061. doi:10.1074/jbc.M109.052969

Kimelberg, H. K., & Nedergaard, M. (2010). Functions of astrocytes and their potential as therapeutic targets. *Neurotherapeutics, 7*(4), 338-353. doi:10.1016/j.nurt.2010.07.006

Kleim, J. A., Cooper, N. R., & VandenBerg, P. A. (2002). Exercise induces angiogenesis but does not alter movement representations within rat motor cortex. *Brain Res, 934*(1), 1-6.

Kleim, J. A., Hogg, T. M., VandenBerg, P. M., Cooper, N. R., Bruneau, R., & Remple, M. (2004). Cortical synaptogenesis and motor map reorganization occur during late, but not early, phase of motor skill learning. *J. Neurosci., 24*(3), 628-633.

Kleim, J. A., & Jones, T. A. (2008). Principles of experience-dependent neural plasticity: implications for rehabilitation after brain damage. *J. Speech Lang Hear. Res, 51*(1), S225-S239.

Kleim, J. A., Lussnig, E., Schwarz, E. R., Comery, T. A., & Greenough, W. T. (1996). Synaptogenesis and FOS expression in the motor cortex of the adult rat after motor skill learning. *Journal of Neuroscience, 16*(14), 4529-4535.

Klineberg, I., Palla, S., & Trulsson, M. (2014). Contemporary Relevance of Occlusion and Mastication. *International Journal of Prosthodontics, 27*(5), 411-412.

Kumar, A., Kothari, M., Grigoriadis, A., Trulsson, M., & Svensson, P. (2018). Bite or Brain: Implication of sensorimotor regulation and neuroplasticity in oral rehabilitation procedures. *Journal of Oral Rehabilitation*, n/a-n/a. doi:10.1111/joor.12603

Lakschevitz, F., Barashi-Gozal, M., Glogauer, M., Sessle, B. J., & Avivi-Arber, L. (2011). Nociceptive Behaviour Following Dental Extraction and Implant Surgery in Rats *International Association for Dental Research, 1483*

Lanjakornsiripan, D., Pior, B. J., Kawaguchi, D., Furutachi, S., Tahara, T., Katsuyama, Y., . . . Gotoh, Y. (2018). Layer-specific morphological and molecular differences in neocortical astrocytes and their dependence on neuronal layers. *Nat Commun, 9*(1), 1623. doi:10.1038/s41467-018-03940-3

Laskawi, R., Rohlmann, A., Landgrebe, M., & Wolff, J. R. (1997). Rapid astroglial reactions in the motor cortex of adult rats following peripheral facial nerve lesions. *European Archives of Oto-Rhino-Laryngology, 254*(2), 81-85. doi:10.1007/bf01526185

Lazarov, N. E. (2007). Neurobiology of orofacial proprioception. *Brain Res Rev, 56*(2), 362-383. doi:10.1016/j.brainresrev.2007.08.009

Lee, M. K., Han, S. R., Park, M. K., Kim, M. J., Bae, Y. C., Kim, S. K., . . . Ahn, D. K. (2011). Behavioral evidence for the differential regulation of p-p38 MAPK and p-NF-kappaB in rats with trigeminal neuropathic pain. *Mol Pain, 7*, 57. doi:10.1186/1744-8069-7-57

Lee, S., Zhao, Y. Q., Ribeiro-da-Silva, A., & Zhang, J. (2010). Distinctive response of CNS glial cells in oro-facial pain associated with injury, infection and inflammation. *Mol Pain, 6*, 79. doi:10.1186/1744-8069-6-79

Liddelow, S., & Barres, B. (2015). SnapShot: Astrocytes in Health and Disease. *Cell, 162*(5), 1170-1170.e1171. doi:10.1016/j.cell.2015.08.029

Liddelow, S. A., & Barres, B. A. (2017). Reactive Astrocytes: Production, Function, and Therapeutic Potential. *Immunity, 46*(6), 957-967. doi:10.1016/j.immuni.2017.06.006

Linden, R. W. (1990). An update on the innervation of the periodontal ligament. *Eur J Orthod, 12*(1), 91-100.

MacVicar, B. A., & Newman, E. A. (2015). Astrocyte Regulation of Blood Flow in the Brain. *Cold Spring Harbor Perspectives in Biology, 7*(5), a020388. doi:10.1101/cshperspect.a020388

Mao, T., Kusefoglu, D., Hooks, B. M., Huber, D., Petreanu, L., & Svoboda, K. (2011). Long-Range Neuronal Circuits Underlying the Interaction between Sensory and Motor Cortex. *Neuron, 72*(1), 111-123. doi:10.1016/j.neuron.2011.07.029

Marbach, J. J., & Raphael, K. G. (2000). Phantom tooth pain: A new look at an old dilemma. *Pain Medicine, 1*(1), 68-77.

McKeon, A., & Benarroch, E. E. (2018). Glial fibrillary acid protein: Functions and involvement in disease. *Neurology, 90*(20), 925-930. doi:10.1212/wnl.0000000000005534

Melis, M., & Zawawi, K. H. (2015). Occlusal dysesthesia: a topical narrative review. *J Oral Rehabil, 42*(10), 779-785. doi:10.1111/joor.12309

Messlinger, K, , S., A, , B., & Raber, P. (2008). *Anatomy and physiology of pain sensitive cranial structures* (Silberstein, S, L. , R, & e. W. s. h. a. o. h. p. Eds. 8th edn ed.). New York: Oxford University Press.

Miehe, B., Fanghanel, J., Kubein-Meesenburg, D., Nagerl, H., & Schwestka-Polly, R. (1999). Masticatory musculature under altered occlusal relationships - a model study with experimental animals. *Annals of Anatomy-Anatomischer Anzeiger, 181*(1), 37-40. doi:10.1016/s0940-9602(99)80084-3

Miller, S. J., & Rothstein, J. D. (2016). Astroglia in Thick Tissue with Super Resolution and Cellular Reconstruction. *PLoS One, 11*(8), e0160391. doi:10.1371/journal.pone.0160391

Monfils, M. H. (2005). In search of the motor engram: Motor map plasticity as a mechanism for encoding motor experience. *The Neuroscientist, 11*(5), 471-483. doi:10.1177/1073858405278015

Mostafeezur, R. M., Shinoda, M., Unno, S., Zakir, H. M., Takatsuji, H., Takahashi, K., . . . Kitagawa, J. (2014). Involvement of astroglial glutamate-glutamine shuttle in modulation of the jaw-opening reflex following infraorbital nerve injury. *Eur J Neurosci, 39*(12), 2050-2059. doi:10.1111/ejn.12562

Mostafeezur, R. M., Zakir, H. M., Yamada, Y., Yamamura, K., Iwata, K., Sessle, B. J., & Kitagawa, J. (2012). The effect of minocycline on the masticatory movements following the inferior alveolar nerve transection in freely moving rats. *Mol Pain, 8*, 27. doi:10.1186/1744-8069-8-27

Mountcastle, V. B. (1997). The columnar organization of the neocortex. *Brain, 120*, 701-722.

Mullen, R. J., Buck, C. R., & Smith, A. M. (1992). NeuN, a neuronal specific nuclear protein in vertebrates. *Development, 116*(1), 201-211.

Nag, S. (2011). Morphology and properties of astrocytes. *Methods Mol Biol, 686*, 69-100. doi:10.1007/978-1-60761-938-3_3

Nakagomi, T., & Matsuyama, T. (2017). Leptomeninges: a novel stem cell niche with neurogenic potential. *Stem Cell Investig, 4*, 22. doi:10.21037/sci.2017.03.09

Navarro, X., Vivo, M., & Valero-Cabre, A. (2007). Neural plasticity after peripheral nerve injury and regeneration. *Prog Neurobiol, 82*(4), 163-201. doi:10.1016/j.pneurobio.2007.06.005

Neafsey, E. J., Bold, E. L., Haas, G., Hurley-Gius, K. M., Quirk, G., Sievert, C. F., & Terreberry, R. R. (1986). The organization of the rat motor cortex: a microstimulation mapping study. *Brain Res, 396*(1), 77-96.

Newman, E. A. (2003). New roles for astrocytes: regulation of synaptic transmission. *Trends Neurosci, 26*(10), 536-542. doi:10.1016/s0166-2236(03)00237-6

Nixdorf, D. R., Drangsholt, M. T., Ettlin, D. A., Gaul, C., de Leeuw, R., Svensson, P., . . . Ceusters, W. (2012). Classifying orofacial pains: a new proposal of taxonomy based on ontology. *J Oral Rehabil, 39*(3), 161-169. doi:10.1111/j.1365-2842.2011.02247.x

Nixdorf, D. R., John, M. T., Wall, M. M., Fricton, J. R., & Schiffman, E. L. (2010). Psychometric properties of the modified Symptom Severity Index (SSI). *J Oral Rehabil, 37*(1), 11-20. doi:10.1111/j.1365-2842.2009.02017.x

Nixdorf, D. R., Moana-Filho, E. J., Law, A. S., McGuire, L. A., Hodges, J. S., & John, M. T. (2010). Frequency of nonodontogenic pain after endodontic therapy: a systematic review and meta-analysis. *Journal of Endodontics, 36*(9), 1494-1498. doi:10.1016/j.joen.2010.06.020

Nixdorf, D. R., Moana-Filho, E. J., Law, A. S., McGuire, L. A., Hodges, J. S., & John, M. T. (2010). Frequency of persistent tooth pain after root canal therapy: a systematic review and meta-analysis. *J Endod, 36*(2), 224-230. doi:10.1016/j.joen.2009.11.007

Oberheim, N. A., Takano, T., Han, X., He, W., Lin, J. H., Wang, F., . . . Nedergaard, M. (2009). Uniquely hominid features of adult human astrocytes. *J Neurosci, 29*(10), 3276-3287. doi:10.1523/jneurosci.4707-08.2009

Oberheim, N. A., Tian, G. F., Han, X., Peng, W., Takano, T., Ransom, B., & Nedergaard, M. (2008). Loss of astrocytic domain organization in the epileptic brain. *J Neurosci, 28*(13), 3264-3276. doi:10.1523/jneurosci.4980-07.2008

Okada-Ogawa, A., Nakaya, Y., Imamura, Y., Kobayashi, M., Shinoda, M., Kita, K., . . . Iwata, K. (2015). Involvement of medullary GABAergic system in extraterritorial neuropathic pain mechanisms associated with inferior alveolar nerve transection. *Exp Neurol, 267*, 42-52. doi:10.1016/j.expneurol.2015.02.030

Oliet, S. H. R., Piet, R., & Poulain, D. A. (2001). Control of Glutamate Clearance and Synaptic Efficacy by Glial Coverage of Neurons. *Science, 292*(5518), 923-926. doi:10.1126/science.1059162

Paxinos, G. (2004). *Rat nervous system*. San Diego: Elsevier Academic Press.

Pekny, M., & Pekna, M. (2014). Astrocyte reactivity and reactive astrogliosis: costs and benefits. *Physiol Rev, 94*(4), 1077-1098. doi:10.1152/physrev.00041.2013

Perea, G., & Araque, A. (2005). Properties of synaptically evoked astrocyte calcium signal reveal synaptic information processing by astrocytes. *J Neurosci, 25*(9), 2192-2203. doi:10.1523/jneurosci.3965-04.2005

Perea, G., Yang, A., Boyden, E. S., & Sur, M. (2014). Optogenetic astrocyte activation modulates response selectivity of visual cortex neurons in vivo. *Nat Commun, 5*. doi:10.1038/ncomms4262

Perez-Alvarez, A., Navarrete, M., Covelo, A., Martin, E. D., & Araque, A. (2014). Structural and functional plasticity of astrocyte processes and dendritic spine interactions. *J Neurosci, 34*(38), 12738-12744. doi:10.1523/jneurosci.2401-14.2014

Piao, Z. G., Cho, I. H., Park, C. K., Hong, J. P., Choi, S. Y., Lee, S. J., . . . Oh, S. B. (2006). Activation of glia and microglial p38 MAPK in medullary dorsal horn contributes to tactile hypersensitivity following trigeminal sensory nerve injury. *Pain, 121*(3), 219-231. doi:10.1016/j.pain.2005.12.023

Pigolkin Yu, I., Chertok, V. M., & Motavkin, P. A. (1985). Age characteristics of the efferent innervation of the pia mater arteries in the human brain. *Neurosci Behav Physiol, 15*(4), 343-350.

Polycarpou, N., Ng, Y. L., Canavan, D., Moles, D. R., & Gulabivala, K. (2005a). Prevalence of persistent pain after endodontic treatment and factors affecting its occurrence in cases with complete radiographic healing. *Int Endod J, 38*(3), 169-178. doi:10.1111/j.1365-2591.2004.00923.x

Polycarpou, N., Ng, Y. L., Canavan, D., Moles, D. R., & Gulabivala, K. (2005b). Prevalence of persistent pain after endodontic treatment and factors affecting its occurrence in cases with complete radiographic healing. *International Endodontic Journal, 38*(3), 169-178.

Power, R. M., & Huisken, J. (2017). A guide to light-sheet fluorescence microscopy for multiscale imaging. *Nature Methods, 14*(4), 360-373. doi:10.1038/nmeth.4224

Pun, H., Awamleh, L., Lee, J. C., & Avivi-Arber, L. (2016). Decreased face primary motor cortex (face-M1) excitability induced by noxious stimulation of the rat molar tooth pulp is dependent on the functional integrity of medullary astrocytes. *Exp Brain Res, 234*(3), 645-657. doi:10.1007/s00221-015-4448-9

Quintana, F. J. (2017). Astrocytes to the rescue! Glia limitans astrocytic endfeet control CNS inflammation. *J Clin Invest, 127*(8), 2897-2899. doi:10.1172/jci95769

Remple, M. S., Bruneau, R. M., VandenBerg, P. M., Goertzen, C., & Kleim, J. A. (2001). Sensitivity of cortical movement representations to motor experience: evidence that skill learning but not strength training induces cortical reorganization. *Behav Brain Res, 123*(2), 133-141.

Renton, T. (2011). Persistent Pain after Dental Surgery. *Rev Pain, 5*(1), 8-17. doi:10.1177/204946371100500103

Richardson, D. S., & Lichtman, J. W. (2015). Clarifying Tissue Clearing. *Cell, 162*(2), 246-257. doi:10.1016/j.cell.2015.06.067

Roberts, E. (1986). What do GABA neurons really do? They make possible variability generation in relation to demand. *Exp Neurol, 93*(2), 279-290.

Rodriguez, J. J., Olabarria, M., Chvatal, A., & Verkhratsky, A. (2009). Astroglia in dementia and Alzheimer's disease. *Cell Death Differ, 16*(3), 378-385. doi:10.1038/cdd.2008.172

Salter, M. W. (2004). Cellular neuroplasticity mechanisms mediating pain persistence. *J Orofac Pain, 18*(4), 318-324.

Sarnat, H. B., Nochlin, D., & Born, D. E. (1998). Neuronal nuclear antigen (NeuN): a marker of neuronal maturation in early human fetal nervous system. *Brain Dev, 20*(2), 88-94.

Selchow O, H. J. (Producer). (2013). Light sheet fluorescence microscopy and revolutionary 3D analyses of live specimens. Retrieved from https://www.zeiss.com/content/dam/Microscopy/Products/imaging-systems/Lightsheet%20Z1/photonik_intl_2013_01_044_HiRes.pdf

Seminowicz, D. A., Laferriere, A. L., Millecamps, M., Yu, J. S. C., Coderre, T. J., & Bushnell, M. C. (2009). MRI structural brain changes associated with sensory and emotional function in a rat model of long-term neuropathic pain. *Neuroimage, 47*(3), 1007-1014. doi:10.1016/j.neuroimage.2009.05.068

Sessle, B., Avivi-Arber, L., & Murray, G. (2013). Motor Control of Masticatory Muscles. In L. K. McLoon & F. Andrade (Eds.), *Craniofacial Muscles* (pp. 111-130): Springer New York.

Sessle, B. J. (2000a). Acute and chronic craniofacial pain: brainstem mechanisms of nociceptive transmission and neuroplasticity, and their clinical correlates. *Crit Rev Oral Biol Med, 11*(1), 57-91.

Sessle, B. J. (2000b). Acute and chronic craniofacial pain: Brainstem mechanisms of nociceptive transmission and neuroplasticity, and their clinical correlates. *Critical Reviews in Oral Biology & Medicine, 11*(1), 57-91.

Sessle, B. J. (2006a). Mechanisms of oral somatosensory and motor functions and their clinical correlates. *Journal of Oral Rehabilitation, 33*(4), 243-261. doi:10.1111/j.1365-2842.2006.01623.x

Sessle, B. J. (2006b). Mechanisms of oral somatosensory and motor functions and their clinical correlates*. *J Oral Rehabil, 33*(4), 243-261. doi:10.1111/j.1365-2842.2006.01623.x

Sessle, B. J. (2007). Glia: non-neural players in orofacial pain. *J Orofac Pain, 21*(3), 169-170.

Sessle, B. J., Avivi-Arber, L., & Murray, G. M. (2013). Motor Control of Masticatory Muscles. In L. K. McLoon & F. Andrade (Eds.), *Craniofacial Muscles* (pp. 111-130): Springer New York.

Shiraishi, N., Avivi-Arber, L., Zimmerman, A., Kataria, N., Lever, T., Inoue, M., . . . Takahashi, K. (2017). *Analysis of the relationship between oral environmental changes and alternations in mastication/swallowing patterns of rats using 3D videofluoroscopic technique*. Paper presented at the 7th European Society for Swallowing Disorders Congress and World Dysphagia Summit, Barcelona, Spain.

Silvestri, L., Paciscopi, M., Soda, P., Biamonte, F., Iannello, G., Frasconi, P., & Pavone, F. S. (2015). Quantitative neuroanatomy of all Purkinje cells with light sheet microscopy and high-throughput image analysis. *Front Neuroanat, 9*, 68. doi:10.3389/fnana.2015.00068

Sofroniew, M. V., & Vinters, H. V. (2010). Astrocytes: biology and pathology. *Acta Neuropathol, 119*(1), 7-35. doi:10.1007/s00401-009-0619-8

Sood, M., Lee, J.-C., Avivi-Arber, L., Bhatt, P., & Sessle, J. B. (2015). Neuroplastic Changes in the Sensorimotor Cortex Associated with Orthodontic Tooth Movement in Rats. *Journal of Comparative Neurology, 523*(10), 1548-1568.

Spence, R. D., Kurth, F., Itoh, N., Mongerson, C. R. L., Wailes, S. H., Peng, M. S., & MacKenzie-Graham, A. (2014). Bringing CLARITY to EAE. *Multiple Sclerosis Journal, 20*, 241-241.

Stefaniuk, M., Gualda, E. J., Pawlowska, M., Legutko, D., Matryba, P., Koza, P., . . . Kaczmarek, L. (2016). Light-sheet microscopy imaging of a whole cleared rat brain with Thy1-GFP transgene. *Sci Rep, 6*, 28209. doi:10.1038/srep28209

Sun, D., & Jakobs, T. C. (2012). Structural remodeling of astrocytes in the injured CNS. *Neuroscientist, 18*(6), 567-588. doi:10.1177/1073858411423441

Sun, D., Lye-Barthel, M., Masland, R. H., & Jakobs, T. C. (2010). Structural remodeling of fibrous astrocytes after axonal injury. *J Neurosci, 30*(42), 14008-14019. doi:10.1523/jneurosci.3605-10.2010

Svensson, P., Romaniello, A., Arendt-Nielsen, L., & Sessle, B. J. (2003). Plasticity in corticomotor control of the human tongue musculature induced by tongue-task training. *Exp Brain Res, 152*(1), 42-51. doi:10.1007/s00221-003-1517-2

Swanson, L. W. (2004). *Brain maps: Structure of the rat brain* (3rd ed.). Amsterdam: Elsevier Inc.

Syed, A. M., Sindhwani, S., Wilhelm, S., Kingston, B. R., Lee, D. S. W., Gommerman, J. L., & Chan, W. C. W. (2017). Three-dimensional imaging of transparent tissues via metal nanoparticle labeling. *Journal of the American Chemical Society, 139*(29), 9961-9971.

Takata, N., & Hirase, H. (2008). Cortical layer 1 and layer 2/3 astrocytes exhibit distinct calcium dynamics in vivo. *PLoS One, 3*(6), e2525. doi:10.1371/journal.pone.0002525

Tanaka, K., Watase, K., Manabe, T., Yamada, K., Watanabe, M., Takahashi, K., . . . Wada, K. (1997). Epilepsy and exacerbation of brain injury in mice lacking the glutamate transporter GLT-1. *Science, 276*(5319), 1699-1702.

Tomer, R., Ye, L., Hsueh, B., & Deisseroth, K. (2014a). Advanced CLARITY for rapid and high-resolution imaging of intact tissues. *Nat Protoc, 9*(7), 1682-1697. doi:10.1038/nprot.2014.123

Tomer, R., Ye, L., Hsueh, B., & Deisseroth, K. (2014b). Advanced CLARITY for rapid and high-resolution imaging of intact tissues. *Nature Protocols, 9*(7), 1682-1697. doi:10.1038/nprot.2014.123

Trulsson, M., & Essick, G. K. (2004). Mechanosensation. In T. S. Miles, B. Nauntofte, & P. Svensson (Eds.), *Clinical oral physiology* (pp. 165-197). Copenhagen: Quintessence.

Trulsson, M., Van der Bilt, A., Carlsson, G. E., Gotfredsen, K., Larsson, P., Mueller, F., . . . Svensson, P. (2012). From brain to bridge: masticatory function and dental implants. *J Oral Rehabil, 39*(11), 858-877. doi:10.1111/j.1365-2842.2012.02340.x

Trulsson, M., Van der Bilt, A., Carlsson, G. E., Gotfredsen, K., Larsson, P., Muller, F., . . . Svensson, P. (2012). From brain to bridge: masticatory function and dental implants. *Journal of Oral Rehabilitation, 39*(11), 858-877. doi:10.1111/j.1365-2842.2012.02340.x

Tsuboi, Y., Iwata, K., Dostrovsky, J. O., Chiang, C. Y., Sessle, B. J., & Hu, J. W. (2011). Modulation of astroglial glutamine synthetase activity affects nociceptive behaviour and central sensitization of medullary dorsal horn nociceptive neurons in a rat model of chronic pulpitis. *Eur J Neurosci, 34*(2), 292-302. doi:10.1111/j.1460-9568.2011.07747.x

Verkhratsky, A., & Butt, A. (2013). Astroglia. In *Glial Physiology and Pathophysiology* (pp. 105-244): John Wiley & Sons, Ltd.

Verkhratsky, A., & Nedergaard, M. (2018). Physiology of Astroglia. *Physiol Rev, 98*(1), 239-389. doi:10.1152/physrev.00042.2016

Westberg, K. G., & Kolta, A. (2011). THE TRIGEMINAL CIRCUITS RESPONSIBLE FOR CHEWING. In M. Kobayashi, N. Koshikawa, K. Iwata, & J. L. Waddington (Eds.), *Translating Mechanisms of Orofacial Neurological Disorder* (Vol. 97, pp. 77-98).

Whittington, N. C., & Wray, S. (2017). Suppression of Red Blood Cell Autofluorescence for Immunocytochemistry on Fixed Embryonic Mouse Tissue. *Curr Protoc Neurosci, 81*, 2.28.21-22.28.12. doi:10.1002/cpns.35

Wilhelmsson, U., Li, L., Pekna, M., Berthold, C. H., Blom, S., Eliasson, C., . . . Pekny, M. (2004). Absence of glial fibrillary acidic protein and vimentin prevents hypertrophy of

astrocytic processes and improves post-traumatic regeneration. *J Neurosci, 24*(21), 5016-5021. doi:10.1523/jneurosci.0820-04.2004

Wolf, H. K., Buslei, R., Schmidt-Kastner, R., Schmidt-Kastner, P. K., Pietsch, T., Wiestler, O. D., & Blumcke, I. (1996). NeuN: a useful neuronal marker for diagnostic histopathology. *J Histochem Cytochem, 44*(10), 1167-1171.

Xie, Y. F., Zhang, S., Chiang, C. Y., Hu, J. W., Dostrovsky, J. O., & Sessle, B. J. (2007). Involvement of glia in central sensitization in trigeminal subnucleus caudalis (medullary dorsal horn). *Brain Behav Immun, 21*(5), 634-641. doi:10.1016/j.bbi.2006.07.008

Yang, G., Baad-Hansen, L., Wang, K., Xie, Q.-F., & Svensson, P. (2014). A study on variability of quantitative sensory testing in healthy participants and painful temporomandibular disorder patients. *Somatosensory and Motor Research, 31*(2), 62-71. doi:10.3109/08990220.2013.869493

Yao, D., & Sessle, B. J. (2018). Face sensorimotor cortex undergoes neuroplastic changes in a rat model of trigeminal neuropathic pain. *Exp Brain Res, 236*(5), 1357-1368. doi:10.1007/s00221-018-5226-2

Yu, P., Wang, H., Katagiri, Y., & Geller, H. M. (2012). An in vitro model of reactive astrogliosis and its effect on neuronal growth. *Methods Mol Biol, 814*, 327-340. doi:10.1007/978-1-61779-452-0_21

Zhao, P., Waxman, S. G., & Hains, B. C. (2007). Modulation of thalamic nociceptive processing after spinal cord injury through remote activation of thalamic microglia by cysteine cysteine chemokine ligand 21. *J Neurosci, 27*(33), 8893-8902. doi:10.1523/jneurosci.2209-07.2007

Zheng, H., & Rinaman, L. (2015). Simplified CLARITY for visualizing immunofluorescence labeling in the developing rat brain. *Brain Struct Funct*. doi:10.1007/s00429-015-1020-0

Zheng, H. Y., & Rinaman, L. (2016). Simplified CLARITY for visualizing immunofluorescence labeling in the developing rat brain. *Brain Struct Funct, 221*(4), 2375-2383. doi:10.1007/s00429-015-1020-0